Redox Biology 26 (2019) 101263

Contents lists available at ScienceDirect

Redox Biology

journal homepage: www.elsevier.com/locate/redox

Protein tyrosine phosphatase 1b deficiency protects against hepatic fibrosis by modulating nadph oxidases

Inmaculada García García-Ruiz[a,b,c,*], Nerea Blanes Ruiz[a,1], Patricia Rada[a,b,1], Virginia Pardo[a,b,2], Laura Ruiz[a,b,2], Ana Blas-García[d,e], M. Pilar Valdecantos[a,b], Montserrat Grau Sanz[c], José A. Solís Herruzo[c], Ángela M. Valverde[a,b,**]

[a] Instituto de Investigaciones Biomédicas Alberto Sols (CSIC-UAM), 28029, Madrid, Spain
[b] Centro de Investigación Biomédica en Red de Diabetes y Enfermedades Metabólicas Asociadas (CIBERdem), ISCIII, 28029, Madrid, Spain
[c] Laboratorio de Gastroenterología y Hepatología, Instituto de Investigación Hospital 12 de Octubre, Universidad Complutense de Madrid, 28041, Madrid, Spain
[d] Centro de Investigación Biomédica en Red de Enfermedades Hepáticas y Digestivas (CIBERhed), ISCIII, 28029, Madrid, Spain
[e] Departamento de Farmacología, Facultad de Medicina, Universitat de València, Valencia, Spain

ARTICLE INFO

Keywords:
Protein tyrosine phosphatase 1B
Liver fibrosis
NADPH oxidases
Inflammation
Bile duct ligation
Bone marrow transplantation

ABSTRACT

Inflammation is typically associated with the development of fibrosis, cirrhosis and hepatocellular carcinoma. The key role of protein tyrosine phosphatase 1B (PTP1B) in inflammatory responses has focused this study in understanding its implication in liver fibrosis. Here we show that hepatic PTP1B mRNA expression increased after bile duct ligation (BDL), while BDL-induced liver fibrosis was markedly reduced in mice lacking *Ptpn1* ($PTP1B^{-/-}$) as assessed by decreased collagen deposition and α-smooth muscle actin (α-SMA) expression. $PTP1B^{-/-}$ mice also showed a significant increase in mRNA levels of key markers of monocytes recruitment (*Cd68, Adgre1* and *Ccl2*) compared to their wild-type ($PTP1B^{+/+}$) littermates at early stages of injury after BDL. Interestingly, the lack of PTP1B strongly increased the NADPH oxidase (NOX) subunits *Nox1/Nox4* ratio and downregulated *Cybb* expression after BDL, revealing a pro-survival pattern of NADPH oxidase induction in response to liver injury. Chimeric mice generated by transplantation of $PTP1B^{-/-}$ bone marrow (BM) into irradiated $PTP1B^{+/+}$ mice revealed similar hepatic expression profile of NOX subunits than $PTP1B^{-/-}$ mice while these animals did not show differences in infiltration of myeloid cells at 7 days post-BDL, suggesting that PTP1B deletion in other liver cells is necessary for boosting the early inflammatory response to the BDL. $PTP1B^{-/-}$ BM transplantation into $PTP1B^{+/+}$ mice also led to a blockade of TGF-β and α-SMA induction after BDL. *In vitro* experiments demonstrated that deficiency of PTP1B in hepatocytes protects against bile acid-induced apoptosis and abrogates hepatic stellate cells (HSC) activation, an effect ameliorated by NOX1 inhibition. In conclusion, our results have revealed that the lack of PTP1B switches NOX expression pattern in response to liver injury after BDL and reduces HSC activation and liver fibrosis.

1. Introduction

Hepatic fibrosis is a common pathological response of the liver to sustained hepatic injury of different etiologies which triggers the activation of hepatic stellate cells (HSC) and the recruitment of inflammatory cells to the site of injury [1,2]. A wide variety of chronic stimuli have been recognized to cause hepatic fibrosis including drugs, viral infections, as well as cholestatic, autoimmune and metabolic diseases [3]. Cholestatic liver diseases are characterized by the retention of bilirubin and bile salts in the liver and elevations of these metabolites in systemic circulation with a significant impact in different organs' function [4]. Depending on the severity of the biliary obstruction, the liver histology may show diffuse mixed inflammatory cell infiltrates, a variable degree of superimposed cholangitis, active immune-mediated processes and increased number of proliferating small bile ducts, which is referred to as ductal reaction [5,6].

During cholestasis, the biliary tree is damaged and cholangiocytes respond by releasing numerous factors that can activate other liver cell

* Corresponding author. Instituto de Investigaciones Biomédicas Alberto Sols (CSIC-UAM), 28029, Madrid, Spain.
** Corresponding author. Instituto de Investigaciones Biomédicas Alberto Sols (CSIC-UAM), 28029, Madrid, Spain.
E-mail addresses: inmagr86@hotmail.com, igarciaruiz.imas12@h12o.es (I.G. García-Ruiz), avalverde@iib.uam.es (Á.M. Valverde).
[1] Equal contributors.
[2] Equal contributors.

https://doi.org/10.1016/j.redox.2019.101263
Received 1 March 2019; Received in revised form 30 May 2019; Accepted 26 June 2019
Available online 29 June 2019

Abbreviations;

ALT	alanine aminotransferase
AST	aspartate aminotransferase
α-SMA	alpha-smooth muscle actin
BDL	biliary ductular surgery
BM	bone marrow
BMT	bone marrow transplantation
CD68	**C**luster of **D**ifferentiation 68
CM	conditioned medium
DMSO	dimethyl sulfoxide
ECM	extracellular matrix
EDTA	ethylenediaminetetraacetic acid
EGTA	ethylene glycol tetraacetic acid
F4/80	adhesion G protein-coupled receptor E1
HSC	hepatic stellate cells
JNK	c-Jun N-terminal kinase
LPS	lipopolysaccharide
MAPK	mitogen-activated protein kinase
MCP1	monocyte chemo-attractant protein 1
MMPs	metalloproteinases
NOX1	NADPH oxidase 1
NOX4	NADPH oxidase 4
PDGF-β	platelet-derived growth factor beta
PTP1B	protein tyrosine phosphatase 1B
$PTP1B^{+/+}$	wild type mice
$PTP1B^{-/-}$	mice lacking *Ptpn1*
PMSF	phenylmethylsulfonyl fluoride
qRT-PCR	quantitative real-time polymerase chain reaction
SDS-PAGE	sodium dodecyl sulfate polyacrylamide gel electrophoresis
TGF-β	transforming growth factor beta
TIMP	tissue inhibitor of metalloproteinase
TLR	Toll-like receptor

types [7]. Direct impact of bile acids in the hepatocytes also activates a signaling network that promotes hepatic inflammation [8,9]. At the cellular and molecular level, as the bile duct attack progresses, the accumulation of bile compounds drives cholangiocytes and hepatocytes necrosis which, in turn, leads to the release of proinflammatory cytokines that promote neutrophils and F4/80-positive monocytes infiltration [10]. Moreover, during liver injury, activated Kupffer cells, the hepatic resident macrophages, also produce proinflammatory cytokines including tumor necrosis factor-α (TNF-α), interleukin-1β (IL-1β), IL-6, and the chemokine monocyte chemoattractant protein (MCP)-1. The increased expression of the above mentioned cytokines, as well as chemokines, growth factors such as platelet-derived growth factor (PDGF), and profibrogenic stimuli such as transforming growth factor-β (TGF-β), triggers the activation, migration, and proliferation of hepatic stellate cells (HSC) and portal fibroblasts (PF) that transdifferentiate into myofibroblasts leading to progressive portal fibrosis, thereby causing secondary biliary cirrhosis and, ultimately, liver failure and hepatocarcinoma (HCC) [7]. Notably, during progression of cholestatic fibrosis, PF are mostly localized in the portal areas, while HSC are located in the pericentral, sinusoidal, and capsular areas of liver parenchyma [11]. Fibrosis is a dynamic process characterized by progressive accumulation of extracellular matrix (ECM) components, mainly collagen type I, III, and IV, whose excessive deposition distorts normal liver architecture and hepatic functionality [12]; this process being executed by myofibroblasts as ECM-producing cells. Moreover, progression to fibrosis involves decreased activity of matrix metalloproteinases (MMPs) and increased levels of their specific tissue inhibitors (TIMPs) [13].

It has been extensively reported that oxidative stress plays a key role in the development of liver fibrosis. The NOX family of NADPH oxidases (NOXs), involved in the host defense system, includes transmembrane proteins that transport electrons across biological membranes to reduce oxygen to superoxide. Multiple evidences indicate that NOXs play a critical role in the inflammatory response and may contribute to tissue fibrosis via multiple mechanisms [14–17]. In particular, knockdown experiments have revealed that, downstream the TGF-β receptor, NOX4 is necessary for HSC activation as well as for the maintenance of the myofibroblast phenotype [18]. Likewise, it has been reported a beneficial effect of the NOX1/4 inhibitor GKT137831 in attenuating fibrosis and reactive oxygen species (ROS) production in preclinical models of liver fibrosis in mice [19].

Protein tyrosine phosphatase 1B (PTP1B) is an ubiquitous intracellular enzyme that has emerged as a relevant modulator of signaling pathways triggered by activation of the tyrosine kinase receptor superfamily. Its enzymatic activity is regulated by tyrosine phosphorylation, serine phosphorylation and oxidation [20]. Although it is well recognized for its pivotal role in insulin signaling due to its ability to dephosphorylate and inactivate the insulin receptor [21,22], the role of PTP1B has substantially been expanded to a dynamic regulator of multiple signaling networks including those mediated by the Janus kinase/signal transducers and activators of transcription (JAK-STAT), providing a link between metabolism and inflammation [23]. PTP1B expression is induced by metabolic low-grade chronic inflammation *in vivo* [24] and, in this context, global PTP1B-deficient mice are protected against diet- and age-induced obesity and insulin resistance [25,26]. PTP1B is also involved in immune cell signaling, particularly by controlling cytokine-mediated signaling pathways; global PTP1B-deficient mice exhibited an increase in monocytes in the spleen and the bone marrow [27]. On one hand, mice with myeloid-specific deletion of PTP1B are resistant to bacterial lipopolysaccharide-induced endotoxemia and high fat diet-induced inflammation [28] but, on the other, PTP1B-deficient macrophages display an increased proinflammatory phenotype *in vitro* and *in vivo* through up-regulation of activation markers [29]. Of relevance, high levels of PTP1B have been recently reported in fibrotic liver tissues [30]. However, the molecular mechanisms mediated by PTP1B in the setting of liver fibrosis during cholestasis remain largely unknown. Hence, we aim to analyze the role of PTP1B in an experimental mouse model of cholestatic liver damage to define its function in the inflammatory responses and HSC activation, as well as in the cellular cross-talk between hepatocytes and HSC during fibrosis.

2. Materials and methods

2.1. Regeants

Common reagents were obtained from Roche (Darmstadt, Germany) or Sigma-Aldrich (St Louis, MO, USA). Tissue culture dishes were from Falcon (Lincoln Park, NJ, USA) and serum and culture media were from Invitrogen and Gibco (Life Technologies/Thermo Fisher, Madrid, Spain). Taurocholic acid (TCA) and chenodeoxycholic acid (CDCA) were purchased from Sigma-Aldrich. The selective NADPH oxidase 1 (NOX1) inhibitor ML171 was purchased from Tocris (Biogen Científica, Madrid, Spain). Reagents for electrophoresis were from Bio-Rad (Hercules, CA, USA) and Sigma-Aldrich.

2.2. Animal care and fibrosis model

Male and female PTP1B heterozygous mice, maintained on a mixed genetic background (C57BL/6J × 129sv), were intercrossed to yield the three genotypes of mice ($PTP1B^{+/+}$, $PTP1B^{+/-}$ and $PTP1B^{-/-}$) as previously described [26]. In this study, we used 8 to 9-week-old

PTP1B$^{+/+}$ and PTP1B$^{-/-}$ male (4–7 mice per group), housed under 12 h light/dark cycle with free access to food and water. The BDL was performed by laparotomy through a 2-cm midline incision following isoflurane anesthesia. The peritoneal cavity was opened and bile duct was separated carefully from the flanking portal vein and hepatic artery. A 5-0 suture was placed around the bile duct and secured with two surgical knots. Another 5-0 suture was then tied in the same manner immediately near the hilum of the liver. When all knots were fixed, superfluous sutures were removed and the peritoneal cavity was rinsed with a 0.9% NaCl solution. The abdominal wall was closed after hemostasis with 4/0 polyglactin 910 (Vicryl, Ethicon, Somerville, NJ) in two layers and analgesic medication was administered. The sham operation was performed similarly without BDL. The mice received health care according to Spanish and European legislation. All animal experimentation was approved by the CSIC and Comunidad de Madrid Animal Care and Use Committees. Animals were sacrificed on days 3, 7, 12 and 24 after operation and the livers were rapidly harvested for further analysis. A portion of the liver tissue was placed in a 4% p-formaldehyde solution and routinely processed for histological assessment, while the remaining tissue was snap frozen and stored at −80 °C. Plasma levels of alanine aminotransferase (ALT), aspartate aminotransferase (AST), and total bilirubin were determined using a conventional automatic analyzer. Small portions of liver tissue were stored in RNA later (Sigma, St Louis, MO, USA) for analysis of gene expression.

2.3. Cell lines and culture conditions

The human liver cell line HepG2 (European Collection of Animal Cell Cultures (ECACC)) and the immortalized human HSC line LX2 (Millipore, Billerica, MA) were routinely grown in Dulbecco's Modified Eagle's Medium (DMEM) culture medium supplemented with 10% fetal bovine serum (FBS) and antibiotics (100 U/ml penicillin/100 μg/ml streptomycin) at 37 °C in a humidified atmosphere of 5% CO_2.

2.4. HSC and hepatocyte isolation from mice

HSC and hepatocytes were obtained from PTP1B$^{+/+}$ and PTP1B$^{-/-}$ mice. Briefly, HSC were isolated through collagenase-pronase perfusion of livers as described originally by Friedman and Roll [31] with the minor modifications introduced by Rippe and co-workers [32]. A 99% purity of HSC was confirmed by retinoid autofluorescence at 350 nm. The cells were grown in DMEM supplemented with 10% FBS, 1 x NEAA (non-essential amino acids) and antibiotics (100 U/ml penicillin/100 μg/ml streptomycin). The medium was changed 24 h after seeding to remove dead cells and debris.

Primary mouse hepatocytes were isolated by perfusion with collagenase as described [33]. Cells were seeded on 6 or 12-well collagen IV pre-coated plates and cultured in media containing DMEM and Ham's F-12 medium (1:1) with heat-inactivated 10% FBS supplemented with 2 mM glutamine, 15 mM glucose, 20 mM HEPES, 100 U/ml penicillin, 100 μg/ml streptomycin and 1 mM sodium pyruvate (attachment media) and maintained in this medium for 24 h. Then, medium was changed according with the experiments as described in Results and Figure Legends sections.

For analysis of protein and mRNA levels, confluent HSC or PTP1B$^{+/+}$ and PTP1B-deficient hepatocytes were cultured in DMEM-2% FBS for 16 h and then stimulated with 200 μM TCA, 200 μM CDCA, 2 ng/ml TGF-β (TGF-β1, Preprotech), 5 ng/ml PDGF-β (PDGF-BB, Preprotech) or vehicle for the indicated periods of time as described in Results and Figure Legends sections.

For conditioned medium (CM) preparation, hepatocytes were grown until optimal confluence (70–80%) was reached. Cell monolayers were washed twice with phosphate buffered saline (PBS) and replenished with DMEM (2% FBS) for 4 h. Subsequently, cells were incubated with bile acids (TCA or CDCA) or vehicle. After the indicated time-periods, media were removed, filtered (0.22 μm) and added to HSC. Since HSC become activated after culture in plastic dishes in a time-dependent manner, experiments were always performed with cells at the same time-frame of culture with previous administration of CM, bile acids or vehicle for the indicated time-periods.

2.5. Isolation and culture of Kupffer cells

Kupffer cells were obtained from livers of PTP1B$^{+/+}$ and PTP1B$^{-/-}$ mice. For Kupffer cells isolation, the supernatant from the first centrifugation of the hepatocyte isolation protocol was collected and centrifuged twice at 50 × *g* for 5 min to discard the pellet with the remaining hepatocytes. The latest supernatant was centrifuged at 300 × *g* for 5 min at 4 °C and the pellet containing the Kupffer cells was resuspended in attachment media. Kupffer cells were separated by two-step Percoll gradient method. After centrifugation at 800 × *g* for 10 min (with breaks off), Kupffer cells were enriched between 25% and 50% Percoll. Finally, Kupffer cells pellet was washed with PBS, centrifuged twice at 500 × *g* for 10 min at 4 °C to wash out the residual percoll solution, and cells were resuspended in DMEM supplemented with 10% heat inactivated FBS, 100 U/ml penicillin, 100 μg/ml streptomycin and 2 mM glutamine.

2.6. Bone marrow transplantation (BMT)

Eight-to 10-week-old PTP1B$^{+/+}$ recipient male mice were exposed to a dose of 1000 rads (10 Gy) by a cesium g-source before transplantation. One-week prior and 2-weeks post BMT, 100 mg/l neomycin and 10 mg/l polymyxin B sulfate (Sigma-Aldrich) were added to the acidified water. Eight-to 10-week-old male PTP1B$^{+/+}$ or PTP1B$^{-/-}$ donor mice were sacrificed and bone marrow cells were collected from the femurs and tibias by flushing femurs with phosphate-buffered saline as described [29]. Each recipient mouse was injected with about 5–6 x10^6 bone marrow cells by retroorbital injection 4 h after irradiation. The donor/recipient combinations were (PTP1B$^{+/+}$ → PTP1B$^{+/+}$) or (PTP1B$^{-/-}$ → PTP1B$^{+/+}$). Twelve weeks after transplantation, genomic DNA was harvested from liver for use in PCR-based genotyping of PTP1B$^{+/+}$ and PTP1B-deficient alleles.

2.7. Histopathology, immunohistochemistry and serum analysis

Hepatic histology was evaluated on 4-μm sections of 4% p-formaldehyde-fixed liver which were blocked in paraffin wax and stained with Hematoxylin and Eosin (H&E), Masson's Trichrome or Sirius Red. The stage of fibrosis was scored in a blinded manner by an experienced pathologist using a four-point severity scale (0, normal; 1, mild; 2, moderate; 3, severe) for necrosis, inflammatory cell infiltration, bile duct hyperplasia and fibrosis [34]. Bile infarcts were quantified in H&E-stained sections and the percentage of the focal necrosis surface to the whole liver section area was assessed. Liver immunohistochemistry was performed as previously described [26]. Random fields (4 per mice) were chosen for quantification of immunostained positive cells. The antibodies used were anti-F4/80 (MCA497, Serotec), anti-Ly6C (provided by A. Castrillo, CSIC, Spain) and anti-α-SMA (A2547, Sigma).

2.8. siRNA knockdown assays

For transient siRNA transfection, HepG2 or LX2 cells were incubated with Opti-Mem (Gibco/Thermo Fisher, Madrid, Spain). After 4 h in this medium, cells were treated with 50 nM scrambled (sc)- or siRNAs specific for human PTP1B (Dharmacon, Madrid, Spain). Transfection was accomplished with lipofectamine RNAiMAX (Invitrogen/Thermo Fisher, Madrid, Spain) following the instructions of the supplier. After 6 h, the dishes were supplemented with 2 vol of complete medium containing 10% FBS and maintained for an additional 24 h period. Cell viability was ensured after this incubation and the plates were washed twice with PBS and incubated with fresh medium containing 2% FBS.

Cells were used 24 h after this step.

2.9. Preparation of total protein extracts

Total proteins were extracted in ice-cold lysis buffer containing 10 mM Tris-HCl, pH 7.5, 150 mM NaCl, 0.1% SDS, 1 mM EDTA, 1 mM EGTA, 10% glycerol, 10 μg/ml leupeptin, 10 μg/ml aprotinin, 2 μg/ml pepstatin A, 1 mM β-mercaptoethanol and 0.5 mM PMSF. The extracts were vortexed for 30 min at 4 °C and after centrifugation for 20 min at 13.000 × *g*, the supernatants were stored at −20 °C. Protein levels were determined using Bradford reagent (Bio-Rad).

2.10. Western blotting

Proteins were separated in 8–10% SDS-polyacrylamide gel electrophoresis (SDS-PAGE) and transferred onto polyvinylidene fluoride (PVDF) membranes (GE Healthcare). After electrotransfer, membranes were incubated for 1 h with low-fat milk powder (5%) in PBS containing 0.1% Tween-20. Blots were subsequently incubated with the appropriate antibodies against β-actin (A5441, Sigma), α-tubulin (T5168, Sigma), vinculin (sc-73614, Santa Cruz Biotechnology) as loading controls and α-SMA (A2547, Sigma), Type I Collagen (COL1A1) (234167, Calbiochem), Bcl-xL (610211, BD Biosciences), PTP1B (07–088, Merck-Millipore), cleaved caspase-3 (9661, Cell Signaling Technology), phospho-JNK1/2 (4668, Cell Signaling Technology), phospho-p38 MAPK (9211, Cell Signaling Technology), phospho-PDGFR (3161, Cell Signaling Technology) and phospho-AKT (Ser473) (sc-7985-R, Santa Cruz Biotechnology) at the dilutions recommended by the suppliers. Signals were detected using the ECL Western Blotting Detection Reagent (Bio-Rad). Values of densitometry were determined using the Quantity One software (Bio-Rad).

2.11. RNA isolation and real-time quantitative PCR analysis

RNA was extracted with TRIzol Reagent (Invitrogen/Thermo Fisher, Madrid, Spain) and reverse transcribed using Transcriptor First Strand

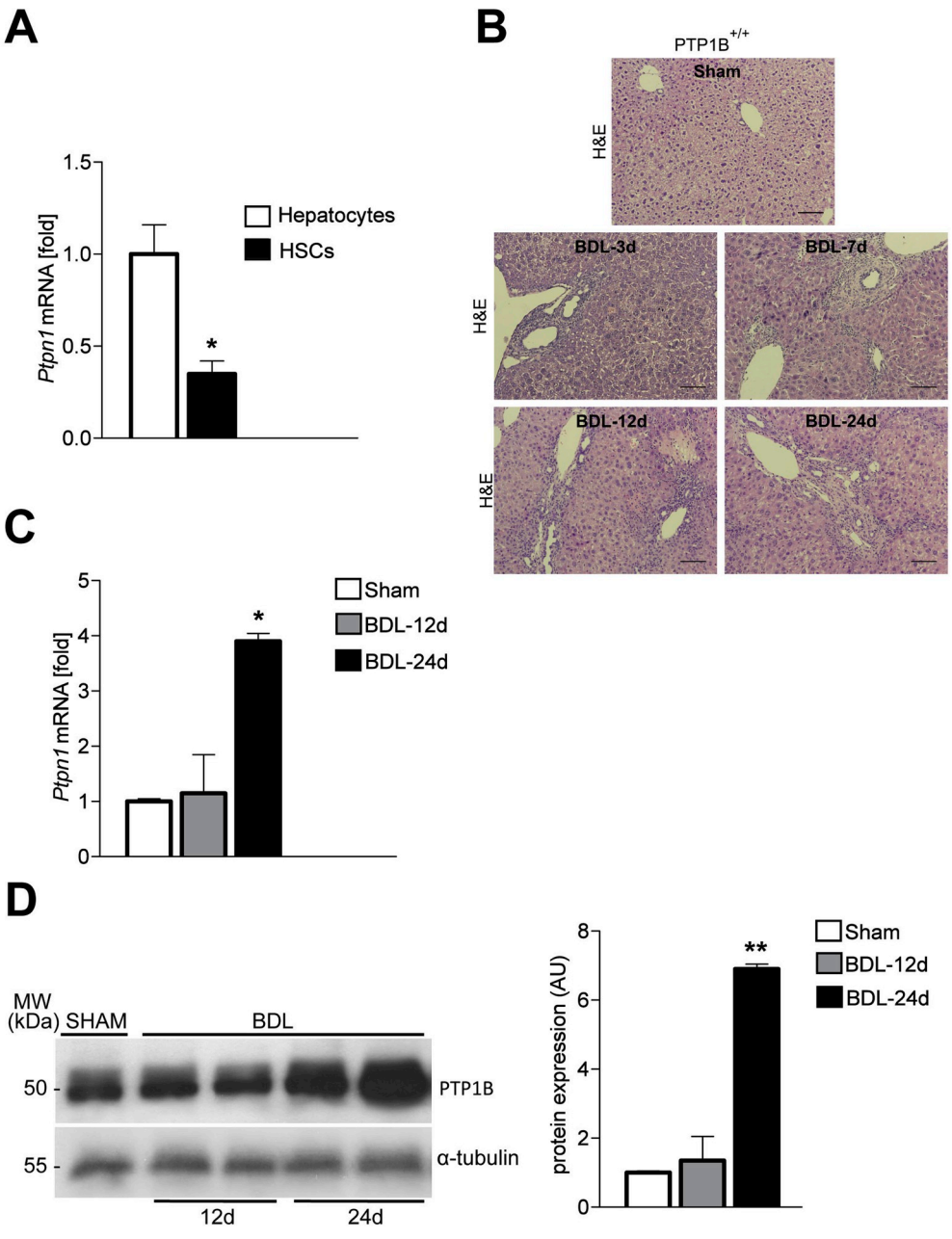

Fig. 1. Evaluation of PTP1B expression following BDL in mouse livers. (A) *Ptpn1* mRNA levels in primary mouse HSC and hepatocytes after normalization to the corresponding expression of *Actb* (n = 4 mice per group). Data are expressed as mean ± SEM. $^{*}P < 0.05$ for primary mouse HSC *versus* primary mouse hepatocytes. **(B)** Representative H&E-stained liver sections in PTP1B$^{+/+}$ mice at different time-periods post BDL. Scale bar = 100 μm Abbreviations: BDL-3d, BDL-7d, BDL-12d and BDL-24d bile duct ligation at 3, 7, 12 and 24 days, respectively; H&E, Hematoxylin and Eosin. **(C)** Hepatic mRNA levels of *Ptpn1* were measured in PTP1B$^{+/+}$ mice after BDL (n = 5 mice per group) at the indicated time-periods by RT-qPCR after normalization to the corresponding expression of *Actb* in total liver RNA. **(D)** PTP1B protein expression in liver extracts was detected by Western blot (n = 5 mice per group). The adjacent bar graph represents the fold change of protein levels after normalization with α-tubulin. The protein expression in the sham-operated group was assumed to be 1. Data in panels C and D are expressed as mean ± SEM. $^{*}P < 0.05$, $^{**}P < 0.01$ for BDL *versus* sham-operated mice.

cDNA Synthesis Kit following the indications of the manufacturer (Roche Diagnostics, Barcelona, Spain). Quantitative real-time polymerase chain reaction (RT-qPCR) was conducted on a Light Cycler 1.0 (Roche Applied Science) in 20 μL final volume with 50 ng of cDNA, 0.5 μM primers, and 2 μL of FastStart DNA Master SYBR Green I (Roche Applied Science, Mannheim, Germany) as previously described [35]. The sequence of primers is available upon request. Gene expression was normalized to that corresponding to *Actb* (encoding β-Actin).

2.12. Statistical analysis

All statistical analyses were carried out using SPSS for Windows, Version 21.0 (SPSS Inc. IBM, Amonk, NY, USA). Results are expressed as the mean ± standard error of the mean (SEM). For comparisons between groups, one-way ANOVA with posthoc Bonferroni's correction was used except for Figs. 1A, 5B and 5C, 5D, 5E, Supplementary Fig. 2 and Supplementary Fig. 3 in which Student's *t*-test was used. P values less than 0.05 were considered statistically significant.

3. Results

3.1. Liver expression of PTP1B is increased during cholestasis and the lack of PTP1B ameliorates BDL-induced liver injury in mice

Since HSC have consistently been shown to play a key role in hepatic fibrogenesis, we first examined PTP1B expression in both freshly isolated HSC and hepatocytes from PTP1B$^{+/+}$ mice. *Ptpn1* mRNA expression in HSC was confirmed by RT-qPCR although with marked lower levels compared to primary hepatocytes (Fig. 1A). Following BDL, PTP1B$^{+/+}$ mouse livers displayed focal necrosis (infarcts) and portal inflammatory changes together with an increase in mostly large bile ducts that was histologically consistent with biliary obstruction (Fig. 1B). Liver gene expression analysis revealed a significant increase in *Ptpn1* mRNA levels 24 days after surgery (Fig. 1C) that highly correlated with PTP1B protein abundance (Fig. 1D). These findings suggest that during BDL-induced cholestatic injury PTP1B levels are up-regulated and may contribute to the progression of biliary injury and hepatic fibrosis.

Because the levels of mRNA encoding *Ptpn1* and PTP1B protein were increased in mouse liver after BDL, studies were conducted to determine the role of this tyrosine phosphatase in the activation of HSC and subsequent development of hepatic fibrosis. To achieve this goal, PTP1B$^{+/+}$ and PTP1B$^{-/-}$ mice were subjected to BDL or sham surgery and livers were analyzed at two time periods (12 and 24 days) post-BDL. Hepatic mRNA levels of *Acta2* and *Col1a1*, encoding α-SMA and Type I Collagen respectively, key markers of HSC cell activation [36,37], were significantly increased in PTP1B$^{+/+}$ mice at 12 and 24 days post-BDL compared to values of their respective PTP1B$^{+/+}$ sham-operated counterparts (Fig. 2A). Likewise, α-SMA and Type I Collagen protein expression was highly increased in the livers of PTP1B$^{+/+}$ mice in a time-dependent manner after BDL (Fig. 2B). On the other hand, basal levels of α-SMA and Type I Collagen were higher in the livers of sham operated PTP1B$^{-/-}$ mice compared to their sham-operated PTP1B$^{+/+}$ counterparts, but the elevation of both HSC markers after BDL was significantly ameliorated (Fig. 2A and B). Immunohistochemistry of liver sections performed at 12 days post-BDL showed α-SMA positive cells localized in both pericentral and portal areas, likely in HSC and PF cells, respectively, in PTP1B$^{+/+}$ mice (Fig. 2C). However, in PTP1B$^{-/-}$ livers α-SMA immunostaining was almost absent in pericentral areas, but it was retained around portal vessels.

In PTP1B$^{+/+}$ mice, the values of both ALT and AST, well-established serum markers of hepatic injury, rapidly increased and peaked at day 3 after BDL and then decreased steadily until day 24 (Table 1). Besides, PTP1B$^{-/-}$ mice showed significantly less pronounced increases of ALT and AST levels at day 3 post-BDL that assessed attenuated liver damage. In line with the cholestatic injury, plasma levels of total bilirubin were abnormal in BDL operated animals of both genotypes indicating that the benefit of PTP1B deficiency in protecting against acute liver injury could not be ascribed to the severity of cholestasis. Predictably, there was no difference in these parameters between sham-operated control groups at the different time periods analyzed and, therefore, these data were pooled (Table 1). In both genotypes, liver-to-body weight ratio was significantly increased at 12 and 24 days after BDL suggesting edema, liver hyperplasia and ductular proliferation as reported [38].

Hepatic fibrosis is a critical endpoint reflecting chronic injury conditions. Development of liver fibrosis was semi-quantitatively analyzed based on the liver histology. Twenty-four days after BDL, PTP1B$^{+/+}$ mice presented significant hepatic fibrosis determined by Masson's Trichrome and Sirius Red staining of liver sections (Fig. 2D, Supplementary Fig. 1). By contrast, PTP1B$^{-/-}$ mice showed diminished fibrosis as demonstrated by reduced collagen deposition. The differences in the fibrogenic response after BDL were also assessed by the analysis of *Tgfb* and *Timp1* mRNA expression which was significantly elevated after 12 ($P < 0.05$, $P < 0.01$, respectively) and 24 ($P < 0.01$) days of the BDL in PTP1B$^{+/+}$ mice in comparison with their sham-operated controls (Fig. 2E). Of note, induction of TIMP-1 expression strongly promotes ongoing fibrotic development by inhibiting MMPs enzymes involved in ECM catabolism [39]. In agreement with the liver histology, the elevations in both markers were reduced in the livers from PTP1B-deficient mice at both time periods after BDL as compared with their sham-operated counterparts and also were significantly lower compared with the elevations of PTP1B$^{+/+}$ mice.

3.2. PTP1B deficiency results in an early proinflammatory response after BDL

At day 3 post-BDL, infiltration of inflammatory cells into the liver tended to be more pronounced in PTP1B$^{-/-}$ than in PTP1B$^{+/+}$ mice although without reaching statistical significance (Fig. 3A); however, at day 7 post-BDL the absence of PTP1B was significantly associated with increased liver inflammation. Since the inhibition of PTP1B exacerbates the proinflammatory responses [29], and based on the above results showing that PTP1B$^{-/-}$ mice exhibited increased inflammatory cells infiltration after BDL, we investigated immune responses in this mouse model at 3 and 7 days post-BDL. First, recruited monocytes and resident macrophages during cholestasis-mediated liver damage was assessed. The analysis of hepatic mRNA levels of *Ccl2* (encoding MCP1), *Cd68,* and *Adgre1* (encoding F4/80) revealed that these markers were highly elevated in the livers of PTP1B$^{-/-}$ mice at both time periods (Fig. 3B). Immunostaining and quantification of liver sections with anti-F4/80 and anti-Ly6C antibodies at 7 days post-BDL showed that both resident macrophages and recruited inflammatory myeloid cells were more elevated in the livers of PTP1B$^{-/-}$ mice compared to the wild-type (F4/80: 166.60 ± 8.52 PTP1B$^{+/+}$ *versus* 304.60 ± 20.72 PTP1B$^{-/-}$; $P = 0.0011$ and Ly6C: 16.27 ± 3.38 PTP1B$^{+/+}$ *versus* 58.89 ± 10.67 PTP1B$^{-/-}$; $P = 0.0005$). In addition, perforin (*Prf1*), granzyme b (*Gzmb*) and lysozyme 6G (*Ly6G*) mRNA levels were measured as markers of Natural Killer (NK) cells, CD8 T cells and neutrophil populations, respectively, and in this case neither substantial elevations compared to myeloid markers nor differences between the two genotypes were found. We then examined whether the lack of PTP1B specifically affected M1 or M2 macrophages during development of liver injury after BDL by analyzing M1 (iNOS, IL-1β) or M2 (IL-4, IL-13) markers. As shown in Fig. 3C, M1 markers were significantly increased in the liver during acute injury while M2 markers were markedly down-regulated. However, gene expression analysis of M1/M2 polarized macrophages in livers did not show significant differences between BDL groups from both genotypes of mice although increased *Nos2* mRNA levels in PTP1B$^{-/-}$ livers was detected (Fig. 3C). Interestingly, as shown in Supplementary Fig. 2 and in agreement with the enhancement

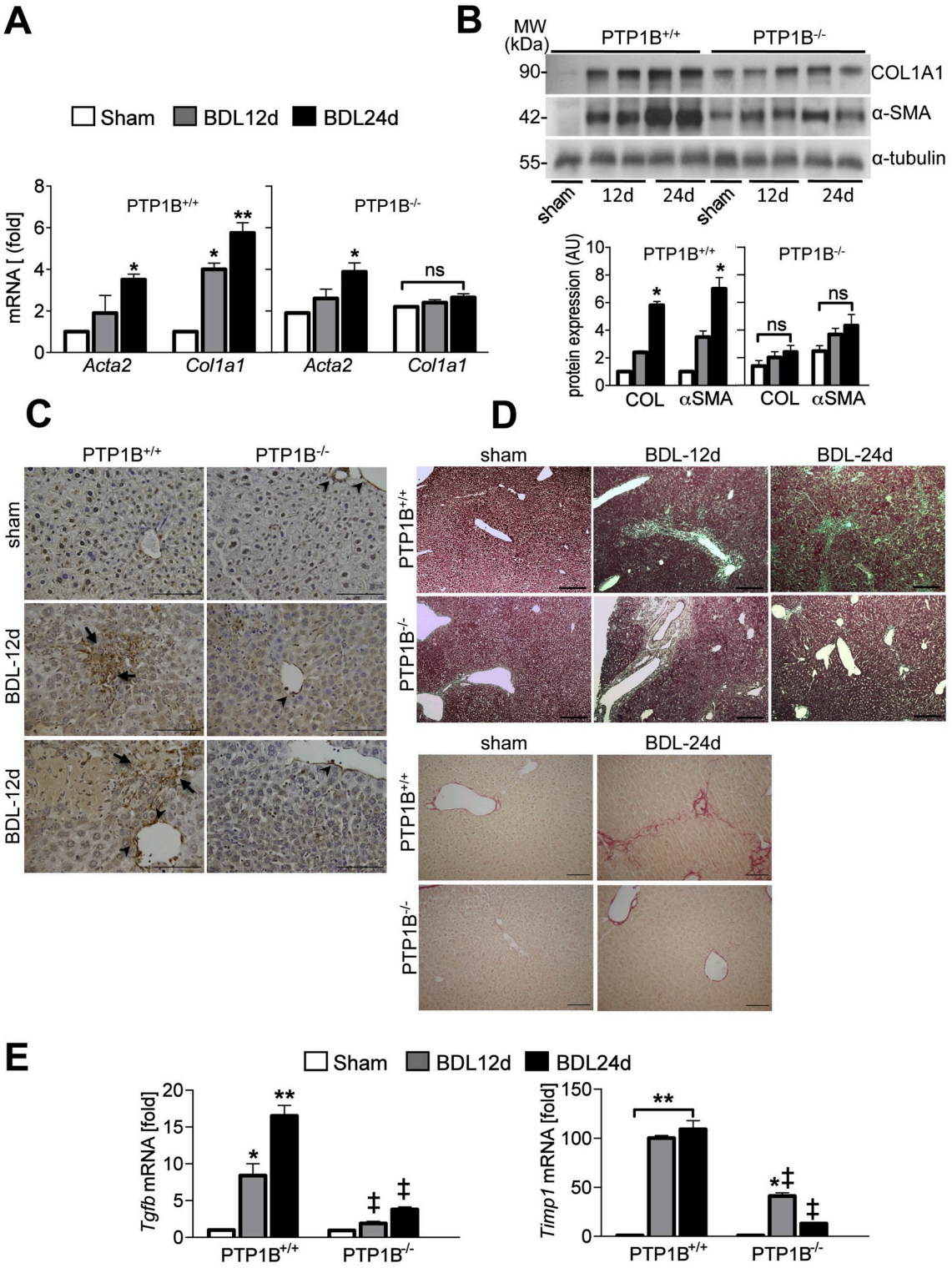

Fig. 2. Decreased fibrogenic markers in livers from PTP1B$^{-/-}$ mice after BDL. PTP1B$^{+/+}$ and PTP1B$^{-/-}$ mice were subjected to sham or BDL surgical procedures and sacrificed at different time-periods. **(A)** Hepatic mRNA levels of *Acta2* and *Col1a1* were measured using RT-qPCR after normalization to the corresponding expression of *Actb*. **(B)** α-SMA and Type I Collagen protein levels were detected by Western blot. Bar graph shows the fold change of protein levels after normalization with α-tubulin. The mRNA and protein expression in the PTP1B$^{+/+}$ sham group were assumed to be 1. Data in **(A)** and **(B)** are expressed as mean ± SEM of 5–7 mice per experimental group and are expressed *versus* their corresponding genotype-matched sham-operated mice. *$P < 0.05$, **$P < 0.01$ for BDL mice *versus* the corresponding PTP1B$^{+/+}$ or PTP1B$^{-/-}$ sham-operated mice. **(C)** Representative images of α-SMA immunostaining in liver sections from sham or 12 days post-BDL operated mice. Immunostaining in pericentral areas is indicated by black arrows while black arrowheads point to α-SMA positive immunostaining in portal areas. Scale bar = 100 μm. **(D)** Representative images of Masson's Trichrome and Sirius Red stained liver sections from PTP1B$^{+/+}$ and PTP1B$^{-/-}$ mice subjected to sham or 12 and 24 days of BDL surgical procedure. Scale bar = 100 μm. **(E)** Hepatic mRNA levels of *Tgfb* and *Timp1* were measured 12 and 24 days after BDL by means of RT-qPCR after normalization to the corresponding expression of *Actb*. In all panels data are expressed as mean ± SEM of 5–7 mice per experimental group. *$P < 0.05$, **$P < 0.01$ for BDL *versus* the corresponding PTP1B$^{+/+}$ or PTP1B$^{-/-}$ sham-operated mice; ‡$P < 0.01$ *versus* BDL PTP1B$^{+/+}$ mice at the indicated time-periods. Abbreviations: ns, non-significant. (For interpretation of the references to colour in this figure legend, the reader is referred to the Web version of this article.)

Table 1
Clinical parameters of PTP1B $^{+/+}$ and PTP1B$^{-/-}$ mice after BDL.

Parameter	Sham		BDL Day 3		BDL Day 7		BDL Day 12		BDL Day 24	
	WT	KO	WT	KO	WT	KO	WT	KO	WT	KO
ALT (U/L)	10 ± 0.6	11 ± 0.6	769 ± 113*	296 ± 17*†	376 ± 62*	326 ± 56*	270.5 ± 8.6	258.3 ± 1.1*	158.8 ± 1.2	161.8 ± 3.6
AST (U/L)	41 ± 0.7	43 ± 1.4	653.2 ± 35*	361 ± 44*	609,8 ± 95*	434.6 ± 12*	420 ± 6.7**	383.2 ± 4.4**	318.3 ± 7.7*	231 ± 13.9*
Liver/body weight (%)	5.6 ± 0.1	5.7 ± 0.1	5.8 ± 0,3	5.8 ± 0,4	6.7 ± 0,6	7.2 ± 0,8	7.4 ± 0.4*	7.5 ± 0.9*	7.7 ± 0.6*	8.2 ± 0.6*
Total bilurrubin(mg/dL)	0.4 ± 0.0	0.4 ± 1.0	4,9 ± 1.3	7.6 ± 3.3	9.3 ± 2.4	10.4 ± 3.7	10.9 ± 3.9	13.4 ± 2.9	15.8 ± 2.6	17.6 ± 1.3

Abbreviations: BDL, bile duct ligation; WT, PTP1B $^{+/+}$ mice; KO, PTP1B$^{-/-}$ mice; ALT, alanine aminotransferase; AP, alkaline phosphatase; AST, aspartate aminotransferase; * $P < 0.05$ and ** $P < 0.01$ from BDL PTP1B$^{+/+}$ or BDL PTP1B$^{-/-}$ versus their corresponding sham-operated mice; † $P < 0.05$ from BDL PTP1B$^{-/-}$ versus BDL PTP1B$^{+/+}$ mice at the respective time-points.

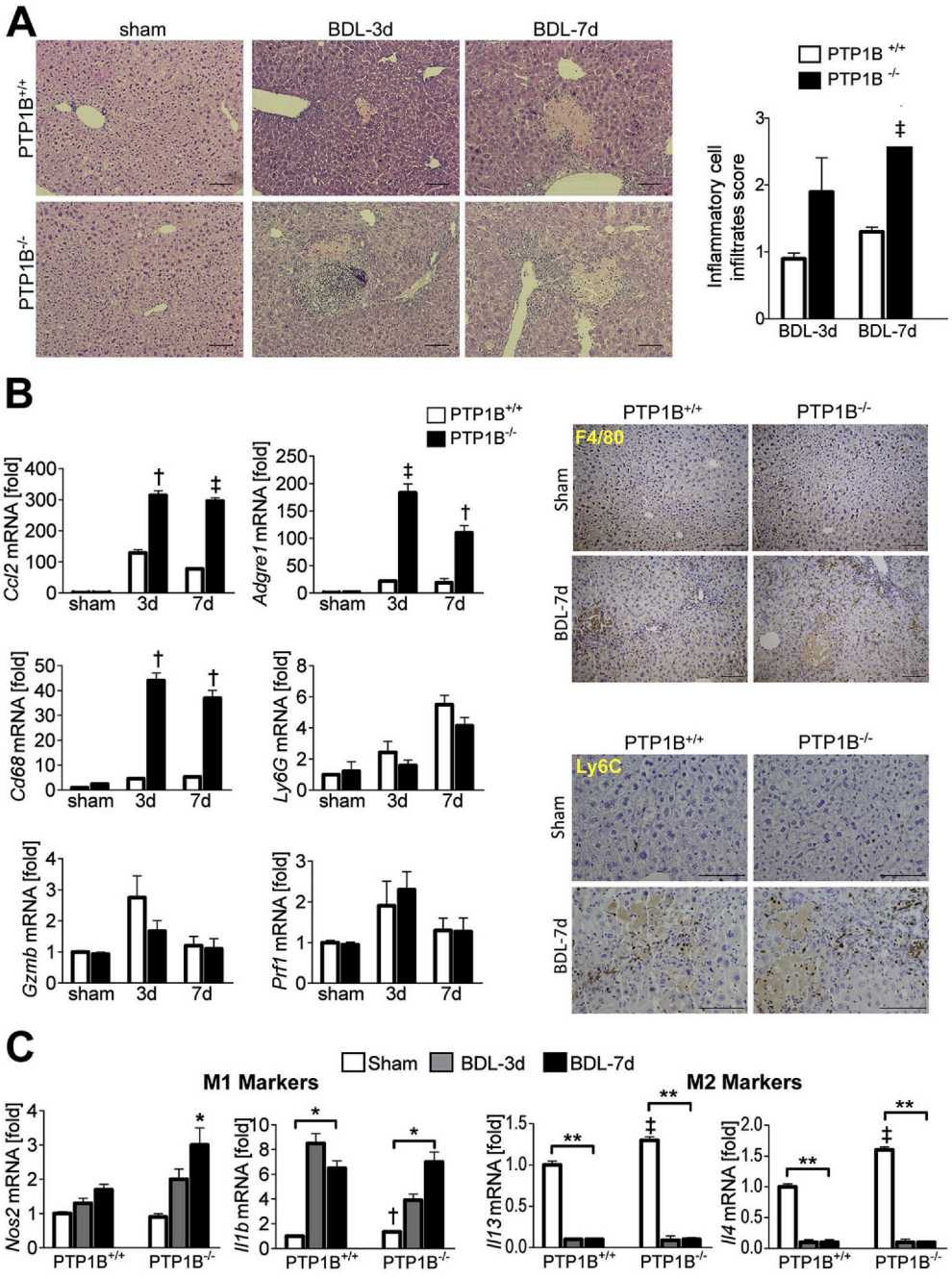

Fig. 3. PTP1B deficiency exacerbates hepatic immune response without modifying the M1/M2 pattern after BDL. (A) Liver damage was assessed by H&E staining in liver sections after 3 and 7 days of BDL in PTP1B$^{+/+}$ and PTP1B$^{-/-}$ mice. Scale bar = 100 μm. Inflammatory cell infiltration was scored as described in Materials and Methods section. **(B)** (*Left panel*) Hepatic mRNA levels of *Ccl2*, *Cd68*, *Adgre1*, *Prf1*, *Gzmb* and *Ly6G* were measured 3 and 7 days after BDL by means of RT-qPCR after normalization to the corresponding expression of *Actb*. (*Right panel*) Representative images of F4/80 and Ly6C immunostaining after 7 days of BDL in PTP1B$^{+/+}$ and PTP1B$^{-/-}$ mice. Scale bar = 100 μM. **(C)** Hepatic mRNA levels of *Nos2*, *Il1b*, *Il13* and *Il14* were measured using RT-qPCR after normalization to the corresponding expression of *Actb*. In all panels data are expressed as mean ± SEM of 5–7 mice per experimental group. *$P < 0.05$, **$P < 0.01$ for BDL mice *versus* the corresponding PTP1B$^{+/+}$ or PTP1B$^{-/-}$ sham-operated mice. †$P < 0.05$, ‡$P < 0.01$ *versus* BDL PTP1B$^{+/+}$ mice at the indicated time-points. Abbreviations: BDL-3d, BDL-7d, bile duct ligation at 3 and 7 days, respectively; H&E, Hematoxylin and Eosin.

of M1 markers in PTP1B$^{-/-}$ macrophages previously reported [29], primary Kupffer cells lacking PTP1B presented higher M1 mRNA levels, an effect also observed in liver samples.

3.3. PTP1B deficiency increases Nox1/Nox4 mRNA ratio and down-regulates Cybb expression after BDL

A previous study showed that the lack of PTP1B promotes an altered NOX expression pattern in hepatocytes in response to TGF-β [40]. Since the NOX family is involved in hepatic myofibroblasts activation and progression of liver fibrosis [41], the expression of NOX enzymes was evaluated in livers of both genotypes after BDL. When we measured *Nox1* and *Nox4* mRNA levels we found their expression differently regulated. While PTP1B-deficient mice showed a non-significant *Nox4* mRNA induction compared to PTP1B$^{+/+}$ mice, mRNA of *Nox1*, related to prosurvival properties [42], was repressed in PTP1B$^{+/+}$ mice at 3 days post-BDL but it was strongly induced in PTP1B$^{-/-}$ mice at all time periods post-BDL analyzed (Fig. 4A). The strong up-regulation of *Nox1* mRNA in PTP1B-deficient mice was further evident in the *Nox1:Nox4* ratio, particularly at the early stages post-BDL (Fig. 4A). Likewise, *Cybb*, encoding the phagocytic NADPH oxidase isoform (NOX2) which plays a key role in HSC activation [43], resulted strikingly opposite regulated in the two genotypes. As shown in Fig. 4B, *Cybb* mRNA significantly increased in livers from PTP1B$^{+/+}$ mice upon BDL reaching a peak at day 3, whereas low levels of *Cybb* expression were detected in livers from PTP1B$^{-/-}$ mice compared with their corresponding sham-operated mice.

3.4. The lack of PTP1B in bone-marrow-derived cells ameliorates BDL-induced liver injury

Macrophages are critical for fibrosis progression and also for its regression because they cannot only exert anti-inflammatory actions, but also degrade ECM proteins [44]. Since we found a significant increase in markers of myeloid inflammatory cells in PTP1B$^{-/-}$ mice after BDL, we investigated the role of PTP1B in the proinflammatory response subsequent to the BDL and its relationship with arresting the progression of liver fibrosis. To achieve this goal, we generated PTP1B-chimeric mice by using a combination of irradiation and bone marrow transplantation (BMT) as described in Materials and Methods. Twelve weeks after transplantation mice were subjected to BDL and sacrificed 7 days later to study the role of BM in both the inflammatory and the fibrogenic expression pattern during hepatic cholestasis. This time point was chosen based on the previous results depicted in Fig. 3A showing substantial differences in immune cells infiltration in the liver between genotypes. BMT was confirmed by PCR-based genotyping of

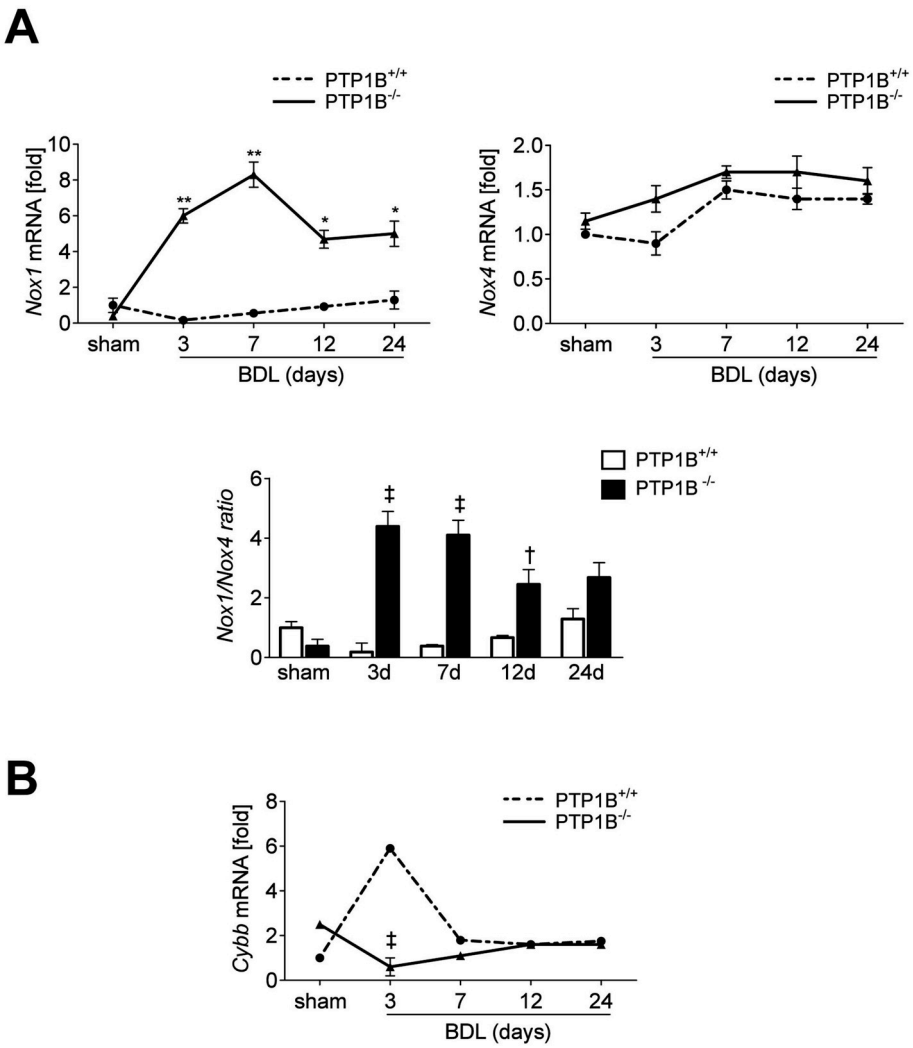

Fig. 4. Differential expression profile of NOX enzymes in response to BDL in PTP1B$^{+/+}$ and PTP1B$^{-/-}$ mice. BDL was performed in PTP1B$^{+/+}$ and PTP1B$^{-/-}$ mice at the indicated time points. **(A)** *Nox1*, *Nox4* and **(B)** *Cybb* expression was determined by RT-qPCR. Values (mean ± SEM from 5 to 7 animals per group) are expressed relative to *Actb*. *$P < 0.05$; **$P < 0.01$ for bile duct-ligated mice *versus* the corresponding PTP1B$^{+/+}$ or PTP1B$^{-/-}$ sham-operated mice. †$P < 0.05$, ‡$P < 0.01$ for bile duct ligated PTP1B$^{+/+}$ mice *versus* bile duct ligated PTP1B$^{-/-}$ mice at each time-point.

PTP1B$^{+/+}$ and PTP1B-deficient alleles in the livers (Fig. 5A) where the transplantation protocol reconstitutes monocyte-derived cells, but not HSC or hepatocytes, with BM-derived cells. By using this approach we generated two types of chimeric mice: PTP1B$^{+/+}$ mice with transplanted PTP1B$^{+/+}$ BM, which contained PTP1B$^{+/+}$ myeloid cells, and PTP1B$^{+/+}$ mice with transplanted PTP1B$^{-/-}$ BM, which contained PTP1B$^{-/-}$ monocytes, hereafter referred as BM^{WT}→WT and BM^{KO}→WT, respectively.

To characterize the evolution of the cholestatic process in transplanted mice, plasma ALT and total bilirubin levels as well as liver-to-body weight ratio were determined in both sham and BDL groups. As expected, plasma bilirubin and ALT were elevated in BDL mice after the cholestatic injury (Fig. 5B) achieving similar peak levels as those reached in BDL mice without transplantation (Table 1); non-significant differences being found among the two experimental groups. Likewise, significant differences in the liver-to-body weight ratio between the two BDL groups were not detected ($P = 0.086$) (Fig. 5B).

Following BMT and BDL, mouse livers showed the typical histological alterations mainly characterized by increased ductular proliferation on portal triads (Fig. 5C). BDL was also associated with increased inflammatory cells infiltration but, unexpectedly, significant differences between the two types of chimeric mice were not found. In BM^{WT} →WT mice, the presence of recruited monocytes and macrophages after BDL was evidenced by the analysis of *Ccl2*, *Cd68* and *Adgre1* mRNA levels (Fig. 5D) together with F4/80 and Ly6C immunostaining (Supplementary Fig. 3). However, BM^{KO} →WT mice did not show the exacerbation of the inflammatory response found in global PTP1B$^{-/-}$ mice post-BDL (Fig. 5C and D and Supplementary Fig. 3). Interestingly, despite the absence of an enhanced immune response, hepatic α-SMA protein content and mRNA levels of *Timp1* were significantly reduced in

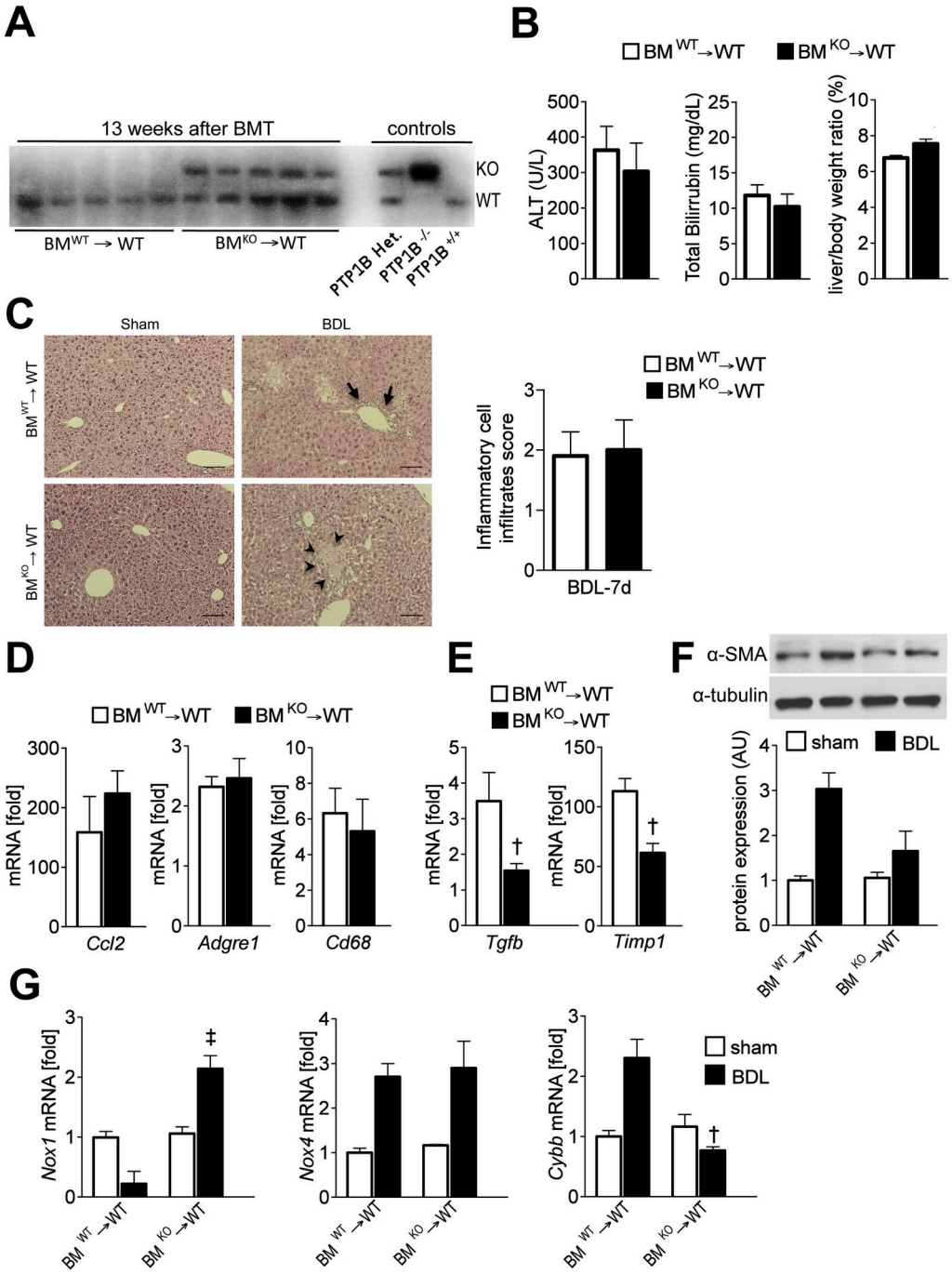

Fig. 5. Transplantation of PTP1B$^{-/-}$ bone marrow into PTP1B$^{+/+}$ mice decreased BDL-induced HSC activation and the pro-fibrotic reaction. PTP1B$^{+/+}$ recipient mice were transplanted with BM from PTP1B$^{+/+}$ or PTP1B$^{-/-}$ donors. Twelve weeks after transplantation, mice were subjected to BDL and sacrificed 7 days later. **(A).** Replenishment of PTP1B$^{-/-}$ deficient macrophages in the liver after BMT was determined by RT-PCR after finishing the BDL protocol. **(B).** Liver function and cholestasis were assessed by the analysis of ALT and total bilirubin plasma levels and liver-to-body weight ratio. **(C).** Representative H&E stained liver sections. BDL mice displayed increased inflammatory cell infiltrates, focal necrosis (infarct) indicated by black arrowheads while black arrows point to bile ducts. Scale bar = 100 μm. Hepatic inflammatory cell infiltration score in livers after BDL is shown in the right panel. **(D).** Liver *Ccl2*, *Adgre1* and *Cd68* mRNA levels were determined by RT-qPCR after normalization to the corresponding expression of *Actb*. **(E).** Transcript levels of *Tgfb andTimp1*. **(F)** α-SMA protein levels in BM^{WT} →WT and BM^{KO} →WT mice. **(G).** mRNA levels of *Nox1*, *Cybb* and *Nox4* in the liver of chimeric mice determined by RT-qPCR after normalization to the corresponding expression of *Actb*. In all panels data represent mean ± SEM and †, ‡, denote *P* values of < 0.05 and < 0.01, respectively, *versus* BDL BM^{WT}→WT mice (n = 5 mice per group). Abbreviations: WT, PTP1B$^{+/+}$; Het, PTP1B$^{+/-}$; KO, PTP1B$^{-/-}$; H&E, Hematoxylin and Eosin.

livers from BM^{KO}→WT mice that correlated with diminished *Tgfb* mRNA levels compared to BM^{WT} →WT mice (Fig. 5E and F), suggesting that the exacerbation of the inflammatory response detected in global $PTP1B^{-/-}$ mice after BDL could not be an absolute requirement for amelioration of liver fibrosis. BMT also resulted in no detectable changes in *Prf1*, *Gzmb* and *Ly6G* mRNA levels between the two

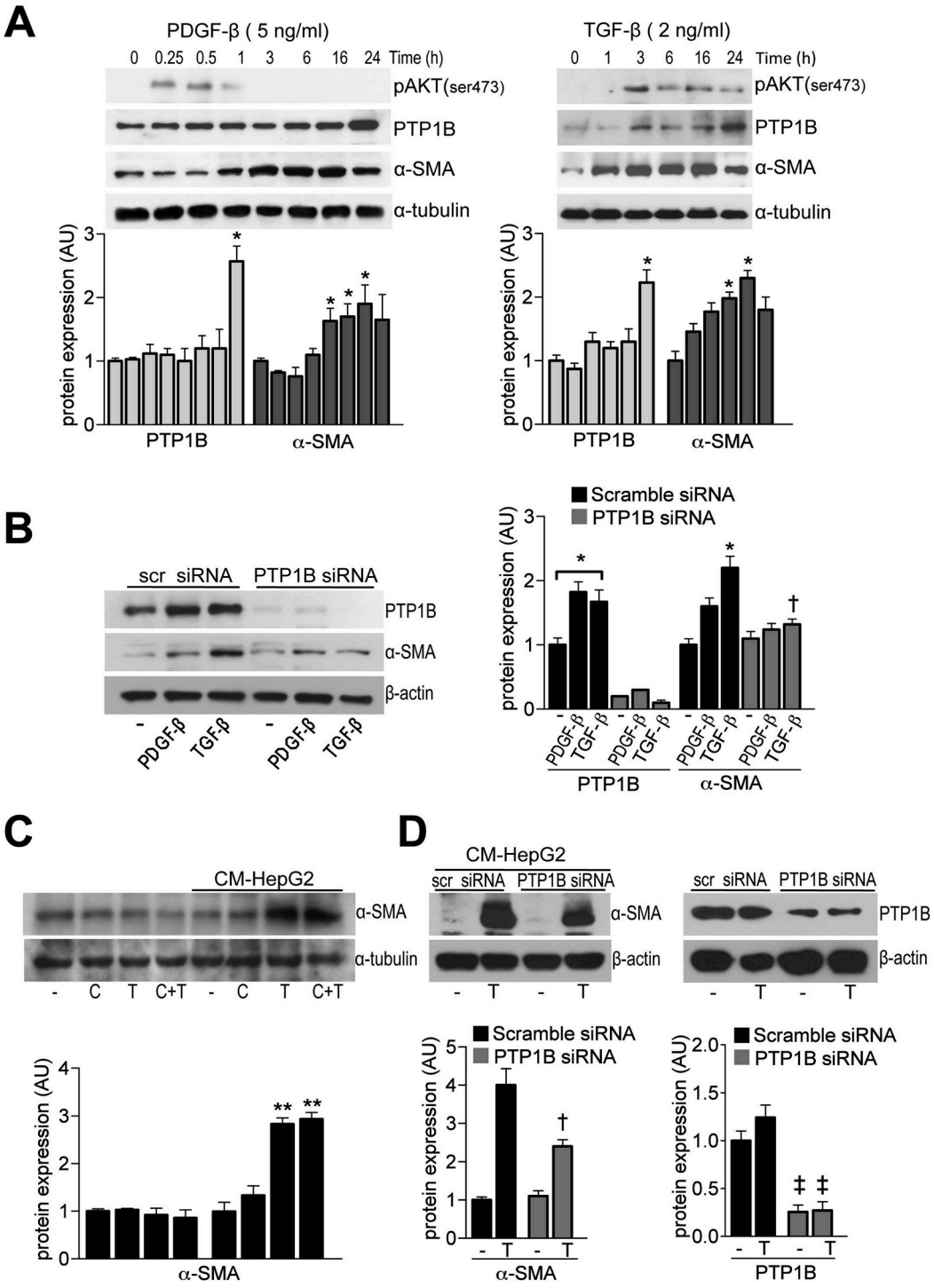

Fig. 6. The presence of PTP1B in hepatocytes and HSC contribute to HSC activation. (A) LX2 cells were stimulated with TGF-β (2 ng/ml) or PDGF-β (5 ng/ml) for different time-periods. Protein levels of PTP1B, α-SMA and *p*-AKT (Ser473) were assessed by Western blot using α-tubulin as loading control. $^{*}P < 0.05$ *versus* untreated cells. **(B)** PTP1B siRNA in LX2 cells decreased their activation upon treatment with TGF-β-or PDGF-β for 24 h as shown by the protein levels of α-SMA analyzed by Western blot using β-actin as loading control. $^{*}P < 0.05$ *versus* untreated cells. †$P < 0.05$ PTP1B siRNA *versus* scrambled (scr)-siRNA group. **(C)** Conditioned medium (CM) from HepG2 cells treated during 8 h with 200 μM TCA or 200 μM CDCA alone or combined was used to treat HSC for 24 h. α-SMA protein levels were analyzed by Western blot using α-tubulin as loading control. Because CDCA needs to be solved in DMSO, 0.02% DMSO final concentration was added to the cell culture medium as vehicle (control condition). $^{**}P < 0.01$ *versus* untreated cells. **(D)** PTP1B siRNA in HepG2 cells diminished TCA-mediated LX2 activation. CM from HepG2 cells treated during 8 h with 200 μM TCA was used to treat LX2 cells for 24 h. α-SMA protein levels analyzed by Western blot using β-actin as loading control. Cell medium was used as vehicle (control condition). †$P < 0.05$, ‡$P < 0.01$ for PTP1B siRNA *versus* scrambled (scr)-siRNA group. In all panels representative Western blots of at least 3 independent experiments are shown. Abbreviations: (−), vehicle; T, Taurocholic acid; C, Chenodeoxicholic acid.

genotypes of mice (Supplementary Fig. 4). On the other hand, NOXs expression pattern was also significantly altered in BM^{KO} →WT mice (Fig. 5G) in line with the results found in global $PTP1B^{-/-}$ mice, although reaching lower maximal levels (Fig. 4).

3.5. Role of PTP1B in HSC activation induced by PDGF-β and TGF-β

Bearing in mind that HSC are key actors implicated in hepatic fibrogenesis, we carried out *in vitro* experiments to assess the impact of PTP1B deficiency in these liver cells in the progression of liver fibrosis. To verify if PTP1B levels are increased in HSC after their activation, we used LX2 human HSC exposed to PDGF-β or TGF-β, both relevant molecules in the pathogenesis of fibrosis and HSC activation [45,46]. As depicted in Fig. 6A, PTP1B protein levels were significantly increased in LX2 cells treated with PDGF-β (5 ng/ml) or TGF-β (2 ng/ml) for 24 h. In addition, both treatments increased α-SMA protein levels in a time-

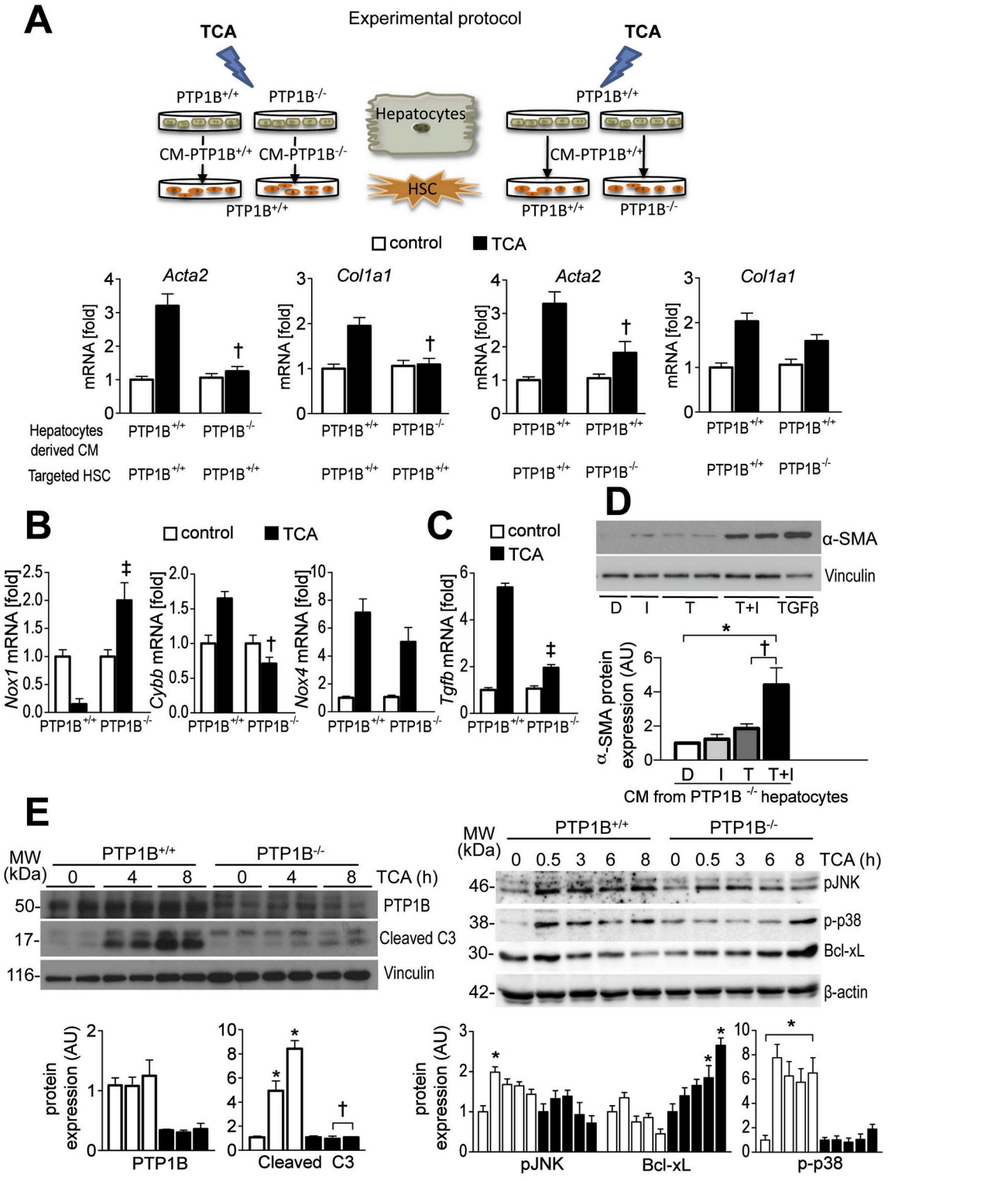

(caption on next page)

Fig. 7. Effects of PTP1B deficiency in hepatocytes in HSC activation after TCA challenge. (A) (*Upper panel*) Scheme of the experimental protocol. *(Lower panel) (left)* HSC isolated from PTP1B$^{+/+}$ mice were exposed for 24 h to the conditioned medium (CM) collected from primary hepatocytes (PTP1B$^{+/+}$ or PTP1B$^{-/-}$) that were treated with 200 μM TCA for 16 h or left untreated *(Lower panel) (right)* HSC isolated from PTP1B$^{+/+}$ or PTP1B$^{-/-}$ mice were exposed during 24 h to the CM collected from PTP1B$^{+/+}$ hepatocytes treated with 200 μM TCA for 16 h or left untreated. *Acta2* and *Col1a1* mRNA levels were determined by RT-qPCR after normalization to the corresponding expression of *Actb*. The mRNA expression in the control group was assumed to be 1. In the left panel †$P < 0.05$ from CM-PTP1B$^{-/-}$ *versus* CM-PTP1B$^{+/+}$. In the right panel †$P < 0.05$, from HSC-PTP1B$^{-/-}$ *versus* HSC-PTP1B$^{+/+}$. RT-qPCR analysis of *Nox1*, *Cybb*, *Nox4* **(B)**, and *Tgfb* **(C)** mRNA levels in hepatocytes untreated or treated with TCA for 16 h †$P < 0.05$, ‡$P < 0.01$ from PTP1B$^{-/-}$ *versus* PTP1B$^{+/+}$ hepatocytes. Values (mean ± S.E.M) are expressed relative to *Actb*. **(D)** α-SMA protein levels in HSC treated with PTP1B$^{-/-}$ hepatocyte-derived CM collected after the treatment with 200 μM TCA in the absence or presence of the NOX1 inhibitor (10 μM) for 16 h. *P < 0.05 *versus* untreated; †P < 0.05 *versus* HSC treated with CM from TCA-treated PTP1B$^{-/-}$ hepatocytes. **(E)** Primary hepatocytes from PTP1B$^{+/+}$ and PTP1B$^{-/-}$ mice were treated with 200 μM TCA for the indicated time-periods. Protein levels of *p*-JNK, p-p38 MAPK, Bcl-xL and the active fragment of caspase-3 were determined by Western blot using β-actin as loading control. *$P < 0.05$ *versus* untreated cells. †$P < 0.05$, from PTP1B$^{-/-}$ *versus* PTP1B$^{+/+}$ hepatocytes. In all panels representative Western blots of at least 3 independent experiments are shown. Abbreviations: CM-PTP1B$^{+/+}$ and CM-PTP1B$^{-/-}$, conditioned medium from PTP1B$^{+/+}$ and PTP1B$^{-/-}$ hepatocytes; HSC-PTP1B$^{+/+}$ and HSC-PTP1B$^{-/-}$, HSC from PTP1B$^{+/+}$ and PTP1B$^{-/-}$ mice; T, Taurocholic acid; D, DMSO; I, NOX1 inhibitor.

dependent manner. Of note, phosphorylation of AKT at Ser 473 was used as positive control to monitor the activation of PDGF-β and TGF-β-mediated signaling. Next, to test whether or not PTP1B was implicated in HSC activation, LX2 cells were transfected with human specific-PTP1B or scrambled siRNAs and, after that, stimulated with either TGF-β or PDGF-β for a further 24 h. As shown in Fig. 6B, PTP1B knockdown significantly decreased α-SMA expression in LX2 cells upon TGF-β or PDGF-β challenge, supporting the implication of this phosphatase in the activation of HSC during liver fibrogenesis. As expected, phosphorylation levels of AKT were significantly increased in PTP1B-silenced LX2 cells stimulated with PDGF-β (Supplementary Fig. 5).

3.6. Conditioned medium from PTP1B-deficient hepatocytes treated with bile acids reduced HSC activation

After BDL, hepatic accumulation of bile acids causes cholestatic hepatocyte injury triggering a hepatocyte-specific inflammatory response that ultimately leads to HSC activation [9]. Accordingly, we determined whether bile acids increase α-SMA by assessing the capacity of hepatocyte-derived conditioned medium (CM) to induce HSC activation. To achieve this, HepG2 cells were treated for 8 h with taurocholic (TCA) and/or chenodeoxycholic (CDCA) acid, two bile acids of interest in the cholestatic injury whose serum levels have been found elevated in mice after BDL [47]. Then, LX2 cells were exposed to the CM collected from bile acid (C for CDCA, T for TCA and C + T for the combination of both bile acids)-stimulated HepG2 cells (CM-HepG2-C, CM-HepG2-T or CM-HepG2-C + T, respectively). Compared to the CM collected from non-treated cells (referred as CM-HepG2-), exposure of LX2 cells to CM-HepG2-T significantly increased their activation which was monitored by the analysis of α-SMA protein levels. However, CM-HepG2-C only induced a moderate increase in α-SMA, being the effect of the CM-HepG2-C + T similar to that of the CM-HepG2-T (Fig. 6C, lanes 5–8). Of note, LX2 cells directly treated with TCA or CDCA did not induce detectable changes in α-SMA expression (Fig. 6C, lanes 1–4). To unravel the importance of PTP1B in hepatocytes in the interplay with HSC during fibrosis development, LX2 cells were exposed to CM from PTP1B-silenced HepG2 cells treated with TCA for 8 h or left untreated (control condition). As shown in Fig. 6D, silencing PTP1B in HepG2 cells significantly decreased α-SMA protein levels in LX2 cells exposed to CM as compared to the effect of the CM collected from scrambled-siRNA transfected HepG2 cells. As expected, PTP1B-siRNA exposure induced a significant decrease of PTP1B protein levels in HepG2 cells.

3.7. PTP1B deficiency in hepatocytes has a major impact in the cross-talk with HSC mediated by bile acids

To avoid potential siRNA off-target effects, the above results were confirmed in primary cells, either hepatocytes or HSC, isolated from PTP1B$^{+/+}$ and PTP1B$^{-/-}$ mice. First, we isolated HSC from PTP1B$^{+/+}$ mice. After plating, these cells were exposed for 16 h to the CM collected from PTP1B$^{+/+}$ or PTP1B$^{-/-}$ hepatocytes that were previously treated with TCA for 16 h (CM-PTP1B$^{+/+}$ or CM-PTP1B$^{-/-}$, respectively) or left untreated as a control (see experimental protocol in Fig. 7A). After gene expression analysis, we found that mRNA levels of fibrosis markers (*Acta2, Col1a1*) were markedly increased in HSC exposed to CM-PTP1B$^{+/+}$ whereas this effect was attenuated in HCS exposed to CM-PTP1B$^{-/-}$ (Fig. 7A, left panel).

To evaluate a direct role of PTP1B expression in HSC in their response to signals released by the hepatocytes, we isolated HSC from PTP1B$^{+/+}$ or PTP1B$^{-/-}$ mice. After plating, the two genotypes of HSC were exposed for 16 h to the CM from PTP1B$^{+/+}$ primary hepatocytes treated with TCA for 16 h or left untreated as a control. As shown in Fig. 7A (right panel), exposure of PTP1B$^{-/-}$ HSC to CM from PTP1B$^{+/+}$ primary hepatocytes treated with TCA (CM-PTP1B$^{+/+}$) caused a moderate decrease in *Acta2* and *Col1a1* mRNA levels as compared with the response of PTP1B$^{+/+}$ HSC. Taken together, these data suggest that PTP1B deficiency in hepatocytes leads to a major impact on HSC activation mediated by bile acids.

After exposure to hepatic insults, oxidative stress is produced through the activation of NOX enzymes in hepatocytes [41]. To study the mRNA expression levels of NOX family members after TCA treatment, primary mouse hepatocytes used to generate the CM were also tested to further explore the expression pattern of NOX subunits. As shown in Fig. 7B, primary PTP1B$^{-/-}$ hepatocytes exposed to TCA for 16 h showed increased *Nox1* mRNA levels compared to PTP1B$^{+/+}$ hepatocytes while an opposite expression pattern in *Cybb* mRNA was observed. Hepatocyte injury after TCA challenge was assessed by the analysis of *Tgfb* mRNA by RT-qPCR. As depicted in Fig. 7C, reduced expression of *Tgfb* mRNA was found in PTP1B$^{-/-}$ hepatocytes (used to generate the CM-PTP1B$^{-/-}$) compared to the levels of PTP1B$^{+/+}$ hepatocytes (used to generate the CM-PTP1B$^{+/+}$), a response coincident with the lower HSC activation (Fig. 7A). To establish a link between PTP1B and NOX1, we treated PTP1B$^{-/-}$ hepatocytes with TCA in the absence or presence of a specific NOX1 inhibitor previously described [48]. After 16 h, we collected the hepatocyte-derived CM that was immediately transferred to mouse HSC. The analysis of αSMA protein levels revealed that the attenuated effect of the CM collected from TCA-stimulated PTP1B$^{-/-}$ hepatocytes in the activation of HSC (Fig. 7A) was abolished in the presence of the NOX1 inhibitor (Fig. 7D). Considering that NOX1 and NOX4 may play different roles in hepatocyte apoptosis [41,42], Western blots analysis was performed in PTP1B$^{+/+}$ and PTP1B$^{-/-}$ hepatocytes after TCA treatment to detect the active caspase 3 subunit, anti-apoptotic Bcl-xL protein levels, as well as the phosphorylation pattern of the kinases JNK and p38 MAPK that participate in pro-apoptotic signaling cascades in response to oxidative stress [49]. As shown in Fig. 7E, PTP1B$^{-/-}$ hepatocytes treated with TCA displayed a significant decrease in pro-apoptotic markers (caspase-3 cleavage and JNK/p38 MAPK phosphorylation) but, on the contrary, these cells presented higher levels of the anti-apoptotic protein Bcl-xL when compared to TCA-stimulated PTP1B$^{+/+}$ cells.

4. Discussion

Cholestatic injury that impairs the flow of bile products from the liver to the duodenum leads to continuous hepatocyte damage and, subsequently, to the development of hepatic fibrosis [4,5,10]. It is well recognized that the activation of HSC and PF is the primary driver of hepatic fibrosis triggered by sustained hepatocyte cell injury and proinflammatory responses associated to cholestasis [2,11]. On one hand, activated HSC produce most of the major and minor ECM proteins of the fibrotic liver [12] and, on the other, during fibrogenesis apoptotic hepatocytes release factors that stimulate the recruitment of inflammatory cells to the site of injury and the activation of BM-derived and liver resident macrophages [1–3]. In addition to the key role of PTP1B in the modulation of the insulin signaling cascade in the liver and its implication in non-alcoholic fatty liver disease, particularly in non-alcoholic steatohepatitis where it has a dual role in its progression and reversion [50], there are several evidences involving this phosphatase in tissue fibrosis. In an acute model, carbon tetrachloride (CCl_4) treatment directly promotes PTP1B accumulation in liver tissue [22], while endothelial PTP1B deletion has been shown to reduce cardiac fibrosis during chronic pressure overload-induced hypertrophy [51]. Likewise, PTP1B deficiency confers resistance against TGF-β-induced apoptosis and growth inhibition in hepatocytes [40]. Of relevance and as it will be discussed below, PTP1B deficiency exacerbates the inflammatory responses [29,52] in different experimental models. Our current study provides evidences of increased PTP1B expression in the fibrotic liver tissue from mice after BDL, as well as in HSC challenged with fibrogenic factors, and further demonstrates that PTP1B deficiency lessens fibrosis in mice and HSC activation *in vivo* and in culture cells. Moreover, positive cells for α-SMA immunostaining were found in both pericentral and portal areas of liver sections from $PTP1B^{+/+}$ mice suggesting that, in addition to HSC, PF are also activated upon BDL. Importantly, in liver sections from $PTP1B^{-/-}$ mice, α-SMA positive cells in pericentral areas were almost absent, suggesting that HSC are major contributors to collagen-producing myofibroblasts as demonstrated by Mederacke and co-workers by an *in vivo* fate tracing approach [53]. It is important to mention that BDL induced a similar degree of cholestasis in $PTP1B^{+/+}$ and $PTP1B^{-/-}$ mice as demonstrated by comparable plasma levels of total bilirubin. However, ALT levels significantly decreased in $PTP1B^{-/-}$ mice 3 days after BDL, suggesting that cholestasis-mediated liver damage requires PTP1B-dependent responses.

The hydrophobic bile acid TCA, which is elevated during cholestasis, seems to exert its fibrogenic actions by activating a signaling network in hepatocytes that likely promotes the release of a secretome that triggers HSC activation. In fact, a direct effect of TCA in promoting the elevation of α-SMA in HSC was not found, supporting the relevance of a cross-talk between hepatocytes and HSC during cholestatic injury. In this regard, CM from TCA-treated hepatocytes increased α-SMA protein content, as well as *Acta2* and *Col1a1* mRNAs in HSC cultures. These responses were markedly attenuated when the CM was collected from TCA-stimulated $PTP1B^{-/-}$ hepatocytes, strongly suggesting that the lack of PTP1B confers protection against cholestatic damage in hepatocytes which, in turn, decreases HSC activation. A possible explanation for these results is based on the protection against apoptotic damage induced by TCA in hepatocytes lacking PTP1B that could lead to a less profibrotic CM. This protective effect of PTP1B deficiency in hepatocytes has been previously reported by our laboratory and others in the context of TNF-α or acetaminophen-mediated liver injury [54,55]. Moreover, supporting the results in mouse hepatic cells, TCA induced less hepatocyte damage in PTP1B silenced human HepG2 cells, as demonstrated by the diminished activation of human HSC exposed to the CM derived from those hepatocytes. However, our results do not exclude a direct effect of PTP1B inhibition in reducing HSC activation since on one hand, HSC isolated from $PTP1B^{-/-}$ mice were partly, but not totally, protected against the deleterious effect of the CM from TCA-treated hepatocytes and, on the other, silencing PTP1B in human LX2 cells conferred protection against the effect of profibrotic molecules such as PDGF-β or TGF-β as recently reported by Chen and co-workers [22].

Regarding the inflammatory process associated with cholestasis, our data show that PTP1B deficiency differentially enhances the activation and recruitment of macrophages in the liver after BDL. We and others have described that PTP1B is an important modulator of macrophages activation, restricting the time of the proinflammatory signaling cascades in response to TLR ligands or IFN [29,52,56,57]. In this context, the results of the present work are in agreement with these studies since after the BDL markers of resident macrophages and recruited monocytes (F4/80, CD68, MCP-1, Ly6C) were elevated in the liver of $PTP1B^{-/-}$ mice. Macrophages play important functional roles in regulating the promotion and resolution of inflammation during fibrosis [44,58]. In fact, macrophage plasticity allows these cells to differentiate into two categories with well-defined phagocitic (M1) or reparative (M2) properties. However, the amelioration of liver damage in $PTP1B^{-/-}$ mice after BDL cannot be ascribed to macrophage polarization because gene expression analysis of M1/M2 markers in the liver did not reveal substantial differences between the two genotypes. Intriguingly, the significant increase of monocytes recruitment into the liver from $PTP1B^{-/-}$ mice at early time periods post-BDL is dispensable for fibrosis resolution since although reconstitution of $PTP1B^{+/+}$-irradiated mice with bone marrow from $PTP1B^{-/-}$ animals did not exacerbate the infiltration of inflammatory cells in the liver as occurred in global $PTP1B^{-/-}$ mice, hepatic α-SMA protein and *Timp1* mRNA levels were significantly reduced in livers from BM^{KO} →WT mice compared to BM^{WT} →WT mice. A possible explanation for these differences could be due, at least in part, to the constitutive basal proinflammatory stage of $PTP1B^{-/-}$ mice, as we previously reported [29]. This proinflammatory priming that confers an advantage for triggering the early phase of liver regeneration after partial hepatectomy [59], could be also relevant to favor an early phagocytic activity after BDL and might be responsible of the increased basal levels of HSC activation markers in livers from PTP1B-deficient mice. In fact, the results of the present study have shown for the first time that proinflammatory markers are constitutively elevated in primary Kupffer cells isolated from $PTP1B^{-/-}$ mice. It also should be mentioned that although it has been demonstrated that after 6 weeks of differentiation in the liver of irradiated and transplanted mice, BM-derived Kupffer cells closely resemble to resident Kupffer cells [60], we cannot exclude that remnant $PTP1B^{+/+}$ Kupffer cells in the liver might attenuate the inflammatory phenotype of BM^{KO}→WT mice. It is also worth noting that due to the extreme sensitivity of $PTP1B^{-/-}$ mice to irradiation [29,57], we were unable to perform BM transplantation in these mice which might have shed light on the importance of PTP1B status in inflammatory *versus* non-inflammatory liver cells in fibrosis progression.

It is well known that ROS are mediators of cell-signaling responses, particularly in pathways involved in protein tyrosine phosphorylation [61]. Accumulating evidences have suggested a critical role for NADPH oxidase, a multi-component enzymatic complex that catalyzes reactions from molecular oxygen to ROS, in the activation process of hepatic myofibroblasts [16,19,62]. Regarding a possible role of NOX family in our *in vivo* experimental model, we found a PTP1B-dependent differential NOX regulation in response to BDL in mice in agreement with data from Ortiz et al. [40]. Thus, deficiency of PTP1B promoted an altered NOX expression pattern in response to cholestatic injury by increasing *Nox1/Nox4* mRNA ratio. Importantly, the same altered NOX pattern was also found in BM^{KO}→WT mice and correlated with diminished *Tgfb* mRNA and α-SMA protein expression after BDL. Nevertheless, BM transplantation did not completely achieve *Nox1* mRNA peak levels detected in global $PTP1B^{-/-}$ mice upon BDL. The later mild phenotype resembles to our previous results [29] pointing to the contribution of other PTP1B-independent NOX sources in this process. Moreover, it should be considered that NOX isoforms are expressed in

the different liver cells. In this regard, HSC and hepatocytes express NOX1, NOX2 and NOX4 that play a key role during HSC activation [41]. Intriguingly, our findings indicate that the three isoforms are also expressed in BM-derived cells in agreement with Picolli et al. [63] since BM transplantation from PTP1B$^{-/-}$ to PTP1B$^{+/+}$ mice is required to achieve the change of NOX expression pattern after BDL. In addition, NOX1 and NOX4 have been described to play opposite roles in the control of cell death and survival as NOX1 knockdown by siRNA increased caspase-3 activity and cell death, whereas NOX4 knockdown attenuated the apoptotic process in hepatocytes [64,65]. Hence, the results found in PTP1B$^{-/-}$ mice suggest a change in the balance between cell death and survival signaling towards a more resistant phenotype compared to the PTP1B$^{+/+}$ mice which concurs with NOX1 upregulation. This effect is also coincident with an opposite modulation of pro- and anti-apoptotic markers in hepatocytes from both genotypes exposed to TCA as previously reported for other pro-apoptotic stimuli [54,55]. Supporting the *in vivo* data, we found that the attenuated effect of the CM derived from TCA-stimulated PTP1B$^{-/-}$ hepatocytes on the activation of HSC was reverted in the presence of a NOX1 inhibitor. On the other hand, the expression of NOX2 protein (encoded by the *Cybb* gene) is increased in the fibrotic liver in mice [66] and a direct evidence of its contribution to hepatic fibrogenesis has been demonstrated by the attenuation of hepatic fibrosis in NOX2-deficient mice compared to wild-type mice after CCl_4 treatment or BDL [67–69]. In this regard, our results also support a role for NOX2 in the phenotype of PTP1B$^{-/-}$ mice since hepatic mRNA levels of *Cybb* were significantly reduced in both PTP1B$^{-/-}$ and transplanted BM^{KO}→WT mice at early time periods post-BDL concurrently with the amelioration of liver damage. Moreover, *Cybb* mRNA was also down-regulated upon TCA challenge in PTP1B$^{-/-}$ hepatocytes compared to their PTP1B$^{+/+}$ counterparts which correlated with a decrease of *Tgfb*, *Acta2* and *Col1a1* mRNA levels. Altogether, our results point to a major impact of PTP1B inhibition in hepatocytes by switching both NOX expression patter and apoptotic/survival pathways in response to bile acids, resulting in the attenuation of HSC activation and fibrosis.

5. Conclusions

In summary, this work suggests the existence of a cross-talk between hepatocytes and HSC in response to cholestatic liver injury that is modulated by PTP1B, being NOX and apoptotic/survival pathways in hepatocytes key drivers in this process. Further work will be necessary to assess the potential role of this novel pathway in therapeutic strategies against hepatic fibrosis.

Authors disclosure statement

None.

Acknowledgements

This work was funded by grants SAF2015-65267-R and RTI2018-094052-B-100 (MICINN/FEDER, Spain), S2017/BMD-3684 MOIR2-CM (Comunidad de Madrid, Spain) and CIBERdem (ISCIII, Spain) to A.M.V; IJCI-2014-19381 (MINECO/FEDER, Spain) to P.R and A.M.V. We also acknowledge H2020 Marie Sklodowska-Curie ITN-TREATMENT (Grant Agreement 721236, European Commission). We acknowledge A. Castrillo (CSIC, Madrid) for his comments and suggestions on the inflammation data.

Appendix A. Supplementary data

Supplementary data to this article can be found online at https://doi.org/10.1016/j.redox.2019.101263.

References

[1] R. Bataller, D.A. Brenner, Liver fibrosis, J. Clin. Investig. 115 (2005) 209–218.
[2] E. Seki, R.F. Schwabe, Hepatic inflammation and fibrosis: functional links and key pathways, Hepatology 61 (2015) 1066–1079.
[3] C. Trautwein, S.L. Friedman, D. Schuppan, M. Pinzani, Hepatic fibrosis: concept to treatment, J. Hepatol. 62 (2015) S15–S24.
[4] M.J. Pollheimer, P. Fickert, B. Stieger, Chronic cholestatic liver diseases: clues from histopathology for patogénesis, Mol. Asp. Med. 37 (2014) 35–56.
[5] P. Ruemmele, F. Hofstaedter, C.M. Gelbmann, Secondary sclerosing cholangitis, Nat. Rev. Gastroenterol. Hepatol. 6 (2009) 287–295.
[6] P. Georgiev, W. Jochum, S. Heinrich, J.H. Jang, A. Nocito, F. Dahm, P.A. Clavien, Characterization of time-related changes after experimental bile duct ligation, Br. J. Surg. 95 (2008) 646–656.
[7] J. Thomson, L. Hargrove, L. Kennedy, J. Demieville, H. Francis, Cellular crosstalk during cholestatic liver injury, Liver Res 1 (2017) 26–33.
[8] S.Y. Cai, X. Ouyang, Y. Chen, C.J. Soroka, J. Wang, A. Mennone, Y. Wang, W.Z. Mehal, D. Jain, J.L. Boyer, Bile acids initiate cholestatic liver injury by triggering a hepatocyte-specific inflammatory response, JCI Insight 2 (2017) e90780.
[9] K. Allen, H. Jaeschke, B.L. Copple, Bile acids induce inflammatory genes in hepatocytes. A novel mechanism of inflammation during obstructive cholestasis, Am. J. Pathol. 178 (2011) 175–186.
[10] A. Kosters, S.J. Karpen, The role of inflammation in cholestasis – clinical and basic aspects, Semin. Liver Dis. 30 (2010) 186–194.
[11] T. Nishio, R. Hu, Y. Koyama, S. Liang, S.B. Rosenthal, G. Yamamoto, D. Karin, J. Baglieri, H.Y. Ma, J. Xu, X. Liu, D. Dhar, K. Iwaisako, K. Taura, D.A. Brenner, T. Kisseleva, Activated Hepatic Stellate Cells and Portal Fibroblasts contribute to cholestatic liver fibrosis in MDR2 knockout mice, J. Hepatol. (2019 May 6), https://doi.org/10.1016/j.jhep.2019.04.012 https://doi.org/10.1016/j.jhep.2019.04.012 pii: S0168-8278(19)30273-9, [Epub ahead of print].
[12] S.L. Friedman, Mechanisms of hepatic fibrogenesis, Gastroenterology 134 (2008) 1655–1669.
[13] J.E. Puche, Y. Saiman, S.L. Friedman, Hepatic stellate cells and liver fibrosis, Comp. Physiol. 3 (2013) 1473–1492.
[14] L. Hecker, R. Vittal, T. Jones, R. Jagirdar, T.R. Luckhardt, J.C. Horowitz, S. Pennathur, F.J. Martinez, V.J. Thannickal, NADPH oxidase-4 mediates myofibroblast activation and fibrogenic responses to lung injury, Nat. Med. 15 (2009) 1077–1081.
[15] I. García-Ruiz, E. Gómez-Izquierdo, T. Díaz-Sanjuán, M. Grau, P. Solís-Muñoz, M.T. Muñoz-Yagüe, J.A. Solís-Herruzo, Sp1 and Sp3 transcription factors mediate leptin-induced collagen α1(I) gene expression in primary culture of male rat hepatic stellate cells, Endocrinology 153 (2012) 5845–5856.
[16] Y.H. Paik, J. Kim, T. Aoyama, S. De Minicis, R. Bataller, D.A. Brenner, Role of NADPH oxidases in liver fibrosis, Antioxidants Redox Signal. 20 (2014) 2854–2872.
[17] E. Crosas-Molista, I. Fabregat, Role of NADPH oxidases in the redox biology of liver fibrosis, Redox Biol 6 (2015) 106–111.
[18] P. Sancho, J. Mainez, E. Crosas-Molist, C. Roncero, C.M. Fernández-Rodriguez, F. Pinedo, H. Huber, R. Eferl, W. Mikulits, I. Fabregat, NADPH oxidase NOX4 mediates stellate cell activation and hepatocyte cell death during liver fibrosis development, PLoS One 7 (2012) e45285.
[19] T. Aoyama, Y.H. Paik, S. Watanabe, B. Laleu, F. Gaggini, L. Fioraso-Cartier, S. Molango, F. Heitz, C. Merlot, C. Szyndralewiez, P. Page, D.A. Brenner, Nicotinamide adenine dinucleotide phosphate oxidase in experimental liver fibrosis: GKT137831 as a novel potential therapeutic agent, Hepatology 56 (2012) 2316–2327.
[20] A. Bourdeau, N. Dube, M.L. Tremblay, Cytoplasmic protein tyrosine phosphatases, regulation and function: the roles of PTP1B and TC-PTP, Curr. Opin. Cell Biol. 17 (2005) 203–209.
[21] M. Elchebly, P. Payette, E. Michaliszyn, W. Cromlish, S. Collins, A.L. Loy, D. Normandin, A. Cheng, J. Himms-Hagen, C.C. Chan, C. Ramachandran, M.J. Gresser, M.L. Tremblay, B.P. Kennedy, Increased insulin sensitivity and obesity resistance in mice lacking the protein tyrosine phosphatase-1B gene, Science 283 (1999) 1544–1548.
[22] P.J. Chen, S.P. Cai, C. Huang, X.M. Meng, J. Li, Protein tyrosine phosphatase 1B (PTP1B): a key regulator and therapeutic target in liver diseases, Toxicology 337 (2015) 10–20.
[23] M.P. Mayers, J.N. Andersen, A. Cheng, M.L. Tremblay, C.M. Horvath, J.P. Parisien, A. Salmeen, D. Barford, N.K. Tonks, TYK2 and JAK2 are substrates of protein-tyrosine phosphatase 1, J. Biol. Chem. 276 (2001) 47771–47774.
[24] J.M. Zabolotny, Y.B. Kim, L.A. Welsh, E.E. Kershaw, B.G. Neel, B.B. Kahn, Protein-tyrosine phosphatase 1B expression is induced by inflammation in vivo, J. Biol. Chem. 283 (2008) 14230–14241.
[25] K.K. Bence, M. Delibegovic, B. Xue, C.Z. Gorgun, G.S. Hotamisligil, B.G. Neel, B.B. Kahn, Neuronal PTP1B regulates body weight, adiposity and leptin action, Nat. Med. 12 (2006) 917-924.
[26] A. González-Rodríguez, J.A. Mas-Gutierrez, M. Mirasierra, A. Fernandez-Perez, Y.J. Lee, H.J. Ko, J.K. Kim, E. Romanos, J.M. Carrascosa, M. Ros, M. Vallejo, C.M. Rondinone, A.M. Valverde, Essential role of protein tyrosine phosphatase 1B in obesity-induced inflammation and peripheral insulin resistance during aging, Aging Cell 11 (2012) 284–296.
[27] K.M. Heinonen, N. Dube, A. Bourdeau, W.S. Lapp, M.L. Tremblay, Protein tyrosine phosphatase 1B negatively regulates macrophage development through CSF-1 signaling, Proc. Natl. Acad. Sci. U.S.A. 103 (2006) 2776–2781.
[28] L. Grant, K.D. Shearer, A. Czopek, E.K. Lees, C. Owen, A. Agouni, J. Workman, C. Martin-Granados, J.V. Forrester, H.M. Wilson, N. Mody, M. Delibegovic,

Myeloid-cell protein Tyrosine Phosphatase-1B deficiency in mice protects against high-fat diet and lipopolysaccharide-induced inflammation, hyperinsulinemia, and endotoxemia through an IL-10 STAT3-dependent mechanism, Diabetes 63 (2014) 456–470.
[29] P.G. Través, V. Pardo, M. Pimentel-Santillana, A. González-Rodríguez, M. Mojena, D. Rico, Y. Montenegro, C. Calés, P. Martín-Sanz, A.M. Valverde, L. Boscá, Pivotal role of protein tyrosine phosphatase 1B (PTP1B) in the macrophage response to pro-inflammatory and anti-inflammatory challenge, Cell Death Dis. 5 (2014) e1125.
[30] P.J. Chen, S.P. Cai, Y. Yang, W.X. Li, C. Huang, X.M. Meng, J. Li, PTP1B confers liver fibrosis by regulating the activation of hepatic stellate cells, Toxicol. Appl. Pharmacol. 292 (2016) 8–18.
[31] S.L. Friedman, F.J. Roll, Isolation and culture of hepatic lipocytes, Kupffer cells, and sinusoidal endothelial cells by density gradient centrifugation with Stractan, Anal. Biochem. 161 (1987) 207–218.
[32] R.A. Rippe, G. Almounajed, D.A. Brenner, Sp1 binding activity increases in activated Ito cells, Hepatology 22 (1995) 241–251.
[33] R. Benveniste, T.M. Danoff, J. Ilekis, H.R. Craig, Epidermal growth factor receptor numbers in male and female mouse primary hepatocyte cultures, Cell Biochem. Funct. 6 (1988) 231–235.
[34] Z.D. Goodman, Grading and staging systems for inflammation and fibrosis in chronic liver diseases, J. Hepatol. 47 (2007) 598–607.
[35] I. García-Ruiz, D. Fernández-Moreira, P. Solís-Muñoz, C. Rodríguez-Juan, T. Díaz-Sanjuán, T. Muñoz-Yagüe, J.A. Solís-Herruzo, Mitochondrial complex I subunits are decreased in murine nonalcoholic fatty liver disease: implication of peroxynitrite, J. Proteome Res. 9 (2010) 2450–2459.
[36] R.K. Moreira, Hepatic stellate cells and liver fibrosis, Arch. Pathol. Lab Med. 131 (2007) 1728–1734.
[37] S.L. Friedman, Mechanisms of disease: mechanisms of hepatic fibrosis and therapeutic implications, Nat. Clin. Pract. Gastroenterol. Hepatol. 1 (2004) 98–105.
[38] M.A. Aller, J.L. Arias, J. García-Domínguez, J.I. Arias, M. Durán, J. Arias, Experimental obstructive cholestasis: the wound-like inflammatory liver response, Fibrogenesis Tissue Repair 1 (2008) 6.
[39] H. Yoshiji, S. Kuriyama, Y. Miyamoto, U.P. Thorgeirsson, D.E. Gomez, M. Kawata, J. Yoshii, Y. Ikenaka, R. Noguchi, H. Tsujinoue, T. Nakatani, S.S. Thorgeirsson, H. Fukui, Tissue inhibitor of metalloproteinases-1 promotes liver fibrosis development in a transgenic mouse model, Hepatology 32 (2000) 1248–1254.
[40] C. Ortiz, L. Caja, E. Bertran, Á. Gonzalez-Rodriguez, A.M. Valverde, I. Fabregat, P. Sancho, Protein-tyrosine phosphatase 1B (PTP1B) deficiency confers resistance to transforming growth factor-β (TGF-β)-induced suppressor effects in hepatocytes, J. Biol. Chem. 287 (2012) 15263–15274.
[41] S. Liang, T. Kisseleva, D.A. Brenner, The role of NADPH Oxidases (NOXs) in liver fibrosis and the activation of myofibroblasts, Front. Physiol. 7 (2016) 17 e Collection.
[42] P. Sancho, E. Bertran, L. Caja, I. Carmona-Cuenca, M.M. Murillo, I. Fabregat, The inhibition of the epidermal growth factor (EGF) pathway enhances TGF-β-induced apoptosis in rat hepatoma cells through inducing oxidative stress coincident with a change in the expression pattern of the NADPH oxidases (NOX) isoforms, Biochim. Biophys. Acta 1793 (2009) 253–263.
[43] J.X. Jiang, S. Venugopal, N. Serizawa, X. Chen, F. Scott, Y. Li, R. Adamson, S. Devaraj, V. Shah, M.E. Gershwin, S.L. Friedman, N.J. Török, Reduced nicotinamide adenine dinucleotide phosphate oxidase 2 plays a key role in stellate cell activation and liver fibrogenesis in vivo, Gastroenterology 139 (2010) 1375–1384.
[44] F. Heymann, C. Trautwein F. Tacke, Monocytes and macrophages as cellular targets in liver fibrosis, Inflamm. Allergy - Drug Targets 8 (2009) 307–318.
[45] P. Czochra, B. Klopcic, E. Meyer, J.F. Garcia-Lazaro, F. Thieringer, P. Schirmacher, S. Biesterfeld, P.R. Galle, A.W. Lohse, S. Kanzler, Liver fibrosis induced by hepatic overexpression of PDGF-B in transgenic mice, J. Hepatol. 45 (2006) 419–428.
[46] I. Fabregat, J. Moreno-Càceres, A. Sánchez, S. Dooley, B. Dewidar, G. Giannelli, TGF-β signalling and liver disease, FEBS J. 282 (2016) 2219–2232.
[47] H.U. Marschall, M. Wagner, K. Bodin, G. Zollner, P. Fickert, J. Gumhold, D. Silbert, A. Fuchsbichler, J. Sjovall, M. Trauner, Fxr(-/-) mice adapt to biliary obstruction by enhanced phase I detoxification and renal elimination of bile acids, J. Lipid Res. 47 (2006) 582–592.
[48] J.S. Moon, K. Nakahira, K.P. Chung, G.M. DeNicola, M.J. Koo, M.A. Pabón, K.T. Rooney, J.H. Yoon, S.W. Ryter, H. Stout-Delgado, NOX4-dependent fatty acid oxidation promotes NLRP3 inflammasome activation in macrophages, Nat. Med. 22 (2016) 1002–1012.
[49] C. Imarisio, E. Alchera, C. Bangalore Revanna, G. Valente, A. Follenzi, E. Trisolini, R. Boldorini, R. Carini, Oxidative and ER stress-dependent ASK1 activation in steatotic hepatocytes and Kupffer cells sensitizes mice fatty liver to ischemia/reperfusion injury, Free Radic. Biol. Med. 112 (2017) 141–148.
[50] A. González-Rodríguez, M.P. Valdecantos, P. Rada, A. Addante, I. Barahona, E. Rey, V. Pardo, L. Ruiz, L.M. Laiglesia, M.J. Moreno-Aliaga, C. García-Monzón, A. Sánchez, A.M. Valverde, Dual role of protein tyrosine phosphatase 1B in the progression and reversion of non-alcoholic steatohepatitis, Mol. Metabol. 7 (2018) 132–146.
[51] R. Gogiraju, M.R. Schroeter, M.L. Bochenek, A. Hubert, T. Munzel, G. Hasenfuss, K. Schafer, Endothelial deletion of protein tyrosine phosphatase-1B protects against pressure overload-induced heart failure in mice, Cardiovasc. Res. 111 (2016) 204–216.
[52] S. Berdnikovs, V.L. Pavlov, H. Abdala-Valencia, C.A. McCary, D.J. Klumpp, M.L. Tremblay, J.M. Cook-Mills, PTP1B deficiency exacerbates inflammation and accelerates leukocyte trafficking in vivo, J. Immunol. 188 (2012) 874–884.
[53] I. Mederacke, C.C. Hsu, J.S. Troeger, P. Huebener, X. Mu, D.H. Dapito, J.P. Pradere, R.F. Schwabe, Fate tracing reveals hepatic stellate cells as dominant contributors to liver fibrosis independent of its aetiology, Nat. Commun. 4 (2013) 2823.
[54] V. Sangwan, G.N. Paliouras, A. Cheng, N. Dube, M.L. Tremblay, M. Park, Protein-tyrosine phosphatase 1B deficiency protects against Fas-induced hepatic failure, J. Biol. Chem. 281 (2006) 221–228.
[55] M.A. Mobasher, A. González-Rodriguez, B. Santamaría, S. Ramos, M.A. Martín, L. Goya, P. Rada, L. Letzig, L.P. James, A. Cuadrado, J. Martín-Pérez, K.J. Simpson, J. Muntané, A.M. Valverde, Protein tyrosine phosphatase 1B modulates GSK3β/Nrf2 and IGFIR signaling pathways in acetaminophen-induced hepatotoxicity, Cell Death Dis. 4 (2013) e626.
[56] C.J. Carbone, H. Zheng, S. Bhattacharya, J.R. Lewis, A.M. Reiter, P. Henthorn, Protein tyrosine phosphatase 1B is a key regulator of IFNAR1 endocytosis and a target for antiviral therapies, Proc. Natl. Acad. Sci. U.S.A. 109 (2012) 19226–19231.
[57] M. Mojena, M. Pimentel-Santillana, A. Povo-Retana, V. Fernández-García, S. González-Ramos, P. Rada, A. Tejedor, D. Rico, P. Martín-Sanz, A.M. Valverde, L. Boscá, Protection against gamma-radiation injury by protein tyrosine phosphatase, Redox Biology 17 (2018) 213–223.
[58] F. Tacke, H.W. Zimmermann, Macrophage heterogeneity in liver injury and fibrosis, J. Hepatol. 60 (2014) 1090–1096.
[59] J. Revuelta-Cervantes, R. Mayoral, S. Miranda, A. González-Rodríguez, M. Fernández, P. Martín-Sanz, A.M. Valverde, Protein tyrosine phosphatase 1B (PTP1B) deficiency accelerates hepatic regeneration in mice, Am. J. Pathol. 178 (2011) 1591–1605.
[60] L. Beattie, A. Sawtell, J. Mann, T.C.M. Frame, B. Teal, F. de Labastida Rivera, N. Brown, K. Walwyn-Brown, J.W.J. Moore, S. MacDonald, E.K. Lim, J.E. Dalton, C.R. Engwerda, K.P. MacDonald, P.M. Kaye, Bone marrow-derived and resident liver macrophages display unique transcriptomic signatures but similar biological functions, J. Hepatol. 65 (2016) 758–768.
[61] A. Salmeen, D. Barford, Functions and mechanisms of redox regulation of cysteine-based phosphatases, Antioxidants Redox Signal. 7 (2005) 560–577.
[62] A. Bettaieb, J.X. Jiang, Y. Sasaki, T.I. Chao, Z. Kiss, X. Chen, J. Tian, M. Katsuyama, C. Yabe-Nishimura, Y. Xi, C. Szyndralewiez, K. Schröder, A. Shah, R.P. Brandes, F.G. Haj, N.J. Török, Hepatocyte NADPH oxidase 4 regulates stress signaling, fibrosis, and insulin sensitivity during development of steatohepatitis in mice, Gastroenterology 149 (2015) 468–480.
[63] C. Piccoli, A. D'Aprile, M. Ripoli, R. Scrima, L. Lecce, D. Boffoli, A. Tabilio, N. Capitanio, Bone marrow derived hematopoietic stem/progenitor cells express multiple isoforms of NADPH oxidase and produce constitutively reactive oxygen species, Biochem. Biophys. Res. Commun. 353 (2007) 965–972.
[64] P. Sancho, I. Fabregat, NADPH oxidase NOX1 controls autocrine growth of liver tumor cells through up-regulation of the epidermal growth factor receptor pathway, J. Biol. Chem. 285 (2010) 24815–24824.
[65] J.X. Jiang, X. Chen, N. Serizawa, C. Szyndralewiez, P. Page, K. Schröder, R.P. Brandes, S. Devaraj, N.J. Török, Liver fibrosis and hepatocyte apoptosis are attenuated by GKT137831 a novel NOX4/NOX1 inhibitor in vivo, Free Radic. Biol. Med. 53 (2012) 289–296.
[66] Y.H. Paik, K. Iwaisako, E. Seki, S. Inokuchi, B. Schnabl, C.H. Osterreicher, T. Kisseleva, D.A. Brenner, The nicotinamide adenine dinucleotide phosphate oxidase (NOX) homologues NOX1 and NOX2/gp91(phox) mediate hepatic fibrosis in mice, Hepatology 53 (2011) 1730–1741.
[67] G. Aram, J.J. Potter, X. Liu, L. Wang, M.S. Torbenson, E. Mezey, Deficiency of nicotinamide adenine dinucleotide phosphate, reduced form oxidase enhances hepatocellular injury but attenuates fibrosis after chronic carbon tetrachloride administration, Hepatology 49 (2009) 911–919.
[68] J.X. Jiang, S. Venugopal, N. Serizawa, X. Chen, F. Scott, Y. Li, R. Adamson, S. Devaraj, V. Shah, M.E. Gershwin, S.L. Friedman, N.J. Torok, Reduced nicotinamide adenine dinucleotide phosphate oxidase 2 plays a key role in stellate cell activation and liver fibrogenesis in vivo, Gastroenterology 139 (2010) 1375–1384.
[69] S.S. Zhan, J.X. Jiang, J. Wu, C. Halsted, S.L. Friedman, M.A. Zern, N.J. Torok, Phagocytosis of apoptotic bodies by hepatic stellate cells induces NADPH oxidase and is associated with liver fibrosis in vivo, Hepatology 43 (2006) 435–443.